Vokrouhlický D., Bottke W. F., Chesley S. R., Scheeres D. J., and Statler T. S. (2015) The Yarkovsky and YORP effects. In *Asteroids IV* (P. Michel et al., eds.), pp. 509–531. Univ. of Arizona, Tucson, DOI: 10.2458/azu_uapress_9780816532131-ch027.

The Yarkovsky and YORP Effects

David Vokrouhlický
Charles University, Prague

William F. Bottke
Southwest Research Institute

Steven R. Chesley
Jet Propulsion Laboratory/California Institute of Technology

Daniel J. Scheeres
University of Colorado

Thomas S. Statler
Ohio University and University of Maryland

The Yarkovsky effect describes a small but significant force that affects the orbital motion of meteoroids and asteroids smaller than 30–40 km in diameter. It is caused by sunlight; when these bodies heat up in the Sun, they eventually reradiate the energy away in the thermal waveband, which in turn creates a tiny thrust. This recoil acceleration is much weaker than solar and planetary gravitational forces, but it can produce measurable orbital changes over decades and substantial orbital effects over millions to billions of years. The same physical phenomenon also creates a thermal torque that, complemented by a torque produced by scattered sunlight, can modify the rotation rates and obliquities of small bodies as well. This rotational variant has been coined the Yarkovsky-O'Keefe-Radzievskii-Paddack (YORP) effect. During the past decade or so, the Yarkovsky and YORP effects have been used to explore and potentially resolve a number of unsolved mysteries in planetary science dealing with small bodies. Here we review the main results to date, and preview the goals for future work.

1. INTRODUCTION

Interesting problems in science usually have a long and complex history. It is rare, though, that they have a prehistory or perhaps even mythology. Yet, until recently this was the case for the Yarkovsky effect. Ivan O. Yarkovsky, a Russian civil engineer born in a family of Polish descent, noted in a privately published pamphlet (*Yarkovsky,* 1901; *Beekman,* 2006) that heating a prograde-rotating planet should produce a transverse acceleration in its motion and thus help to counterbalance the assumed drag from the then-popular ether hypothesis. While this context of Yarkovsky's work was mistaken and he was only roughly able to estimate the magnitude of the effect, he succeeded in planting the seed of an idea that a century later blossomed into a full-fledged theory of how the orbits of small objects revolving about the Sun are modified by the absorption and reemission of solar energy.

It is mainly Ernst J. Öpik who is to be credited for keeping Yarkovsky's work alive and introducing it to western literature, long after the original pamphlet had been lost (*Öpik,* 1951). Curiously, at about the same time, similar ideas also started to appear in Russian regular scientific literature through the works of Vladimir V. Radzievskii and his collaborators (*Radzievskii,* 1952). While Radzievskii was also the first to consider the effects of systematic photon thrust on a body's rotation, his concept was based on a variable albedo coefficient across the surface (*Radzievskii,* 1954). However, there is no strong evidence of large enough albedo variations over surfaces of asteroids or meteoroids. Stephen J. Paddack and John O'Keefe pushed the idea forward by realizing that irregular shape, and thermal radiation rather than just reflected sunlight, will more efficiently change the meteoroid's spin rate. Thence, the Yarkovsky-O'Keefe-Radzievskii-Paddack (YORP) effect was born as an alter ego of the Yarkovsky effect little more than half a century after Yarkovsky's work (see *Paddack* (1969), *Paddack and Rhee* (1975), and *Rubincam* (2000) for a summation of the history and coining of the terminology). Radzievskii's school also briefly touched upon a concept of a radiation-induced acceleration of synchronous planetary satellites (*Vinogradova*

and Radzievskii, 1965), an idea that reappeared much later in a slightly different form as a binary YORP (BYORP) effect (*Ćuk and Burns,* 2005).

The three decades from the 1950s to the 1970s resulted in today's understanding of Yarkovsky and YORP effects. The works that led to a major resurgence in these studies, however, occurred in the second half of the 1990s through the work of David P. Rubincam and Paolo Farinella. Interestingly, both were studying thermal perturbations of artificial satellite motion. With that expertise, they realized a direct link between the orbital effects acting on the artificial satellites such as the Laser Geodynamics Satellites (LAGEOS) and the orbital effects on small meteoroids (e.g., *Afonso et al.,* 1995; *Rubincam,* 1995, 1998; *Farinella et al.,* 1998).

From there, a momentum was gained and a wealth of new results appeared, with applications extending to dynamics of small asteroids and their populations (e.g., *Bottke et al.,* 2002a, 2006). Studies of the Yarkovsky effect were soon followed by those of the YORP effect (*Rubincam,* 2000). Today, both effects belong to a core culture in planetary sciences, as well as beyond (e.g., *http://www.youtube. com/watch?v=kzlgxqXtxYs*), and have become an important part of the agenda of space missions (e.g., *Lauretta et al.,* 2015). Especially after the spectacular discovery of the "once lost" Yarkovsky pamphlet in Russian archives by Dutch amateur astronomer George Beekman (see *Beekman,* 2006), it seems timely to review the current knowledge of the Yarkovsky and YORP effects. This effort could start with a translation, and perhaps a commented edition, of the Yarkovsky work (presently available in its original form as an Appendix to Miroslav Brož's thesis, *http://sirrah. troja.mff.cuni.cz/˜mira/mp/phdth*). We look forward to future historians editing the more than a century long story of the Yarkovsky and YORP effects, with all the known and possibly hidden roots, into a consolidated picture.

Leaving historical issues to their own time, we now turn to current scientific issues related to the Yarkovsky and YORP effects. There are several good technical reviews already existing in the literature (e.g., *Bottke et al.,* 2002a, 2006). While not always possible, we try to avoid discussing the same topics as presented in these previous texts. For instance, we do not review the elementary concepts of the Yarkovsky and YORP effects, assuming the reader is familiar with them. Rather, we try to focus on new results and ideas that emerged during the past decade and that will lead to research efforts in the next several years.

2. THEORY OF THE YARKOVSKY AND YORP EFFECTS

We start with the simplest analytical models of the Yarkovsky and YORP effects (section 2.1). This is because they provide useful insights, such as scalings with several key parameters, and their results are correct to leading order. They also allow us to understand why modeling of the YORP effect is inevitably more complicated than modeling of the Yarkovsky effect. And yet, the quality of the Yarkovsky and YORP effects detections, as well as other applications, have reached a level that requires more accurate models to be used. The first steps toward these new models have been taken recently and these are briefly reviewed in section 2.2.

2.1. Classical Models

2.1.1. The Yarkovsky effect. Absorbed and directly reflected sunlight does not tend to produce long-term dynamical effects as far as orbital motion is concerned (e.g., *Vokrouhlický and Milani,* 2000; *Žižka and Vokrouhlický,* 2011). The Yarkovsky effect thus fundamentally depends on emitted thermal radiation and requires a body to have a nonzero thermal inertia. Any meaningful evaluation of the Yarkovsky effect, therefore, requires a thermophysical model of that body. Fortunately, an evaluation of the Yarkovsky effect imposes a minimum of requirements on the shape of the body; even a simple spherical model provides us with a fair approximation of how the body will orbitally evolve.

While the Yarkovsky effect results in variations to all the orbital elements, what is distinct from most other perturbations is the secular effect in the semimajor axis a, and therefore we only discuss this contribution. Assuming (1) a linearization of the surface boundary condition, (2) a rotation about a spin axis fixed in the inertial space (at least on a timescale comparable with the revolution about the Sun), and (3) a circular orbit about the Sun, one easily finds that the total, orbit-averaged change in a is composed of two contributions (e.g., *Rubincam,* 1995, 1998; *Farinella et al.,* 1998; *Vokrouhlický,* 1998a, 1999), the diurnal effect

$$\left(\frac{da}{dt}\right)_{diurnal} = -\frac{8}{9}\frac{\alpha\Phi}{n} W\left(R_\omega, \Theta_\omega\right) \cos\gamma \qquad (1)$$

and the seasonal effect

$$\left(\frac{da}{dt}\right)_{seasonal} = \frac{4}{9}\frac{\alpha\Phi}{n} W\left(R_n, \Theta_n\right) \sin^2\gamma \qquad (2)$$

Here, $\Phi = \pi R^2 F/(mc)$, where R is the radius of the body, F the solar radiation flux at the orbital distance a from the Sun, m the mass of the body, c the light velocity, n the orbital mean motion, and $\alpha = 1-A$, with A denoting the Bond albedo (e.g., *Vokrouhlický and Bottke,* 2001). The Φ factor is characteristic to any physical effect related to sunlight absorbed or scattered by the surface of the body. Since $m \propto R^3$, one obtains a typical scaling $\Phi \propto 1/R$.

More importantly, the diurnal and seasonal components of the Yarkovsky effect have a different dependence on the spin axis obliquity γ: (1) the diurnal part is $\propto \cos\gamma$, and consequently can make a positive or negative change in the semimajor axis, being maximum at 0° and 180° obliquity values; and (2) the seasonal part is $\propto \sin^2\gamma$, and consequently always results in a decrease in semimajor axis, being

maximum at 90° obliquity. Their magnitude is proportional to the function

$$W\left(R_\nu,\Theta_\nu\right) = -\frac{\kappa_1\left(R_\nu\right)\Theta_\nu}{1+2\kappa_2\left(R_\nu\right)\Theta_\nu+\kappa_3\left(R_\nu\right)\Theta_\nu^2} \qquad (3)$$

determined by the thermal parameters of the body and a frequency ν. The latter is equal either to the rotation frequency ω for the diurnal component, or the orbital mean motion n for the seasonal component. The thermal parameters required by the model are (1) the surface thermal conductivity K, (2) the surface heat capacity C, and (3) the surface density ρ. These parameters, together with the frequency ν, do not appear in equation (3) individually. Rather, in the process of solving the heat diffusion problem and determination of the orbital perturbations, they combine in two relevant parameters. First, they provide a scale length $\ell_\nu = \sqrt{K/(\rho C\nu)}$, which indicates a characteristic penetration depth of temperature changes assuming the surface irradiation is periodic with the frequency ν. The nondimensional radius of the body R_ν in equation (3) is defined by $R_\nu = R/\ell_\nu$. Second, the surface thermal inertia $\Gamma = \sqrt{K\rho C}$ enters the nondimensional thermal parameter Θ_ν in equation (3) using a definition $\Theta_\nu = \Gamma\sqrt{\nu}/(\varepsilon\sigma T_\star^3)$, with ε the thermal emissivity of the surface, σ the Stefan-Boltzmann constant, and $T_\star$ the subsolar temperature ($\varepsilon\sigma T_\star^4 = \alpha F$). When the characteristic size R of the body is much larger than ℓ_ν (a large-body limit), a situation met in the typical applications so far, the three κ coefficients in equation (3) are simply equal to $\frac{1}{2}$ [*Rubincam* (1995); see *Vokrouhlický* (1998a) for their behavior for an arbitrary value of R_ν]. Hence, for large bodies the W factors do not depend on the size R and read $W \simeq W(\Theta_\nu) = -0.5\,\Theta_\nu/(1+\Theta_\nu+0.5\,\Theta_\nu^2)$. Consequently, the Yarkovsky effect is maximum when $\Theta_\nu \simeq 1$; for small or large values of Θ_ν the effect vanishes. In this case, the semimajor axis secular change da/dt due to the Yarkovsky effect scales as $\propto 1/R$ with the characteristic radius R. For small asteroids, either in near-Earth space or in the main belt, Θ_ω is typically on the order of unity (see also the chapter by Delbò et al. in this volume), while Θ_n is much smaller, which implies that the diurnal Yarkovsky component usually dominates the seasonal component.

A handful of models were subsequently developed to probe the role of each of the simplifying assumptions mentioned above using analytical, semianalytical, or fully numerical methods. These include (1) an inhomogeneity of the thermal parameters (e.g., *Vokrouhlický and Brož,* 1999), (2) a coupling of the diurnal and seasonal components of the Yarkovsky effect (e.g., *Vokrouhlický,* 1999; *Sekiya and Shimoda,* 2013, 2014), (3) effects of a nonspherical shape for simple (e.g., *Vokrouhlický,* 1998b) or general geometries (including nonconvex shapes and the role of small-scale surface features; section 2.2), (4) a nonlinearity of the surface boundary condition of the thermal model (e.g., *Sekiya and Shimoda,* 2013, 2014), (5) the role of very high orbital eccentricity (e.g., *Spitale and Greenberg,* 2001, 2002; *Sekiya and Shimoda,* 2014); (6) a nonprincipal-axis rotation state (e.g., *Vokrouhlický et al.,* 2005a), or (7) the Yarkovsky effect for binary asteroids (e.g., *Vokrouhlický et al.,* 2005b). Each of them was found to modify results from the zero approximation model by as much as several tens of percent without modifying the fundamental dependence of the Yarkovsky effect on obliquity, size, or thermal parameters [except perhaps for the special case of very high eccentricity orbits, where the sign of the Yarkovsky effect may be changed (see *Spitale and Greenberg,* 2001)].

2.1.2. The YORP effect. The YORP effect, the rotational counterpart of the Yarkovsky effect, broadly denotes the torque arising from interaction with the impinging solar radiation. As in the orbital effect, the absorbed sunlight does not result in secular effects (e.g. *Breiter et al.,* 2007; *Nesvorný and Vokrouhlický,* 2008b; *Rubincam and Paddack,* 2010). Both directly scattered sunlight in the optical band and the recoil due to thermally reprocessed radiation, however, produce dynamical effects that accumulate over long timescales. In principle, one would need to treat the two components of the YORP effect independently, since the bidirectional characteristics of the scattered and thermally emitted radiation are not the same and would produce different torques. Additionally, the thermal component has a time lag due to the finite value of the surface thermal inertia and its bidirectional function should formally depend on the time history of the particular surface element.

While these issues are at the forefront of current research (section 2.2), we start with a zero-order approximation initially introduced by *Rubincam* (2000): (1) the surface thermal inertia is neglected, such that thermal radiation is reemitted with no time lag; and (2) the reflected and thermally radiated components are simply assumed to be Lambertian (isotropic). This approximation avoids precise thermal modeling and the results are relatively insensitive to the body's surface albedo value. At face value, this looks simple, but layers of complexity unfold with the geometrical description of the surface. This is because the YORP effect vanishes for simple shape models [such as ellipsoids of rotation (*Breiter et al.,* 2007)] and stems from the irregular shape of the body (see *Paddack,* 1969). Obviously, its quantitative description involves a near infinity of degrees of freedom if middle- to small-scale irregularities are included. This may actually be the case for real asteroids because these irregularities may present a large collective cross-section and thus could dominate the overall strength of the YORP effect. This is now recognized as a major obstacle to our ability to model the YORP effect (section 2.2).

The importance of fine details of geometry, somewhat unnoticed earlier, were unraveled by the first analytical and semianalytical models of the YORP effect. There were two approaches developed in parallel. *Scheeres* (2007) and *Scheeres and Mirrahimi* (2008) used the polyhedral shape description as a starting point for their study, while *Nesvorný and Vokrouhlický* (2007, 2008a) and *Breiter and Michałska* (2008) used shape modeling described by a series expansion in spherical harmonics. To keep things simple,

these initial models assumed principal axis rotation and disregarded mutual shadowing of the surface facets. Both models predicted, after averaging the results over the rotation and revolution cycles, a long-term change of the rotational rate ω and obliquity γ (the precession rate effect is usually much smaller than the corresponding gravitational effect due to the Sun), which could be expressed as

$$\frac{d\omega}{dt} = \frac{\Lambda}{C}\sum_{n\geq 1} A_n P_{2n}(\cos\gamma) \quad (4)$$

and

$$\frac{d\gamma}{dt} = \frac{\Lambda}{C\omega}\sum_{n\geq 1} B_n P^1_{2n}(\cos\gamma) \quad (5)$$

Here, $\Lambda = 2\,FR^3/(3c)$ with C being the moment of inertia corresponding to the rotation axis (shortest axis of the inertia tensor), $P_{2n}(\cos\gamma)$ are the Legendre polynomials of even degrees, and $P^1_{2n}(\cos\gamma)$ are the corresponding associated Legendre functions. The particular characteristics of the even-degree Legendre polynomials and Legendre functions on the order of 1 in equations (4) and (5) under prograde to retrograde reflection $\gamma \leftrightarrow \pi-\gamma$ indicate the behavior of dω/dt and dγ/dt: (1) the rotation-rate change is symmetric, while (2) the obliquity change is antisymmetric under this transformation. Earlier numerical studies (e.g., *Rubincam,* 2000; *Vokrouhlický and Čapek,* 2002; *Čapek and Vokrouhlický,* 2004) had suggested that the net effect of YORP on rotation-rate often vanishes near $\gamma \sim 55°$ and $\gamma \sim 125°$. This feature was finally understood using equation (4) because these obliquity values correspond to the roots of the second-degree Legendre polynomial. The previous works that numerically treated smoothed surfaces thus mostly described situations when the first term in the series played a dominant role. When the effects of the surface finite thermal inertia are heuristically added to these models, one finds that only the coefficients B_n change (e.g., *Nesvorný and Vokrouhlický,* 2007, 2008a; *Breiter and Michałska,* 2008). This confirms an earlier numerical evidence of *Čapek and Vokrouhlický* (2004).

Since $C \propto R^5$, equations (4) and (5) imply that both rotation rate and obliquity effects scale with the characteristic radius as $\propto 1/R^2$. This is an important difference with respect to the "more shallow" size dependence of the Yarkovsky effect, and it implies that YORP's ability to change the rotation state increases very rapidly moving to smaller objects. Additionally, we understand well that for very small bodies the Yarkovsky effect becomes eventually nil. When the characteristic radius R becomes comparable to the penetration depth ℓ_ω of the diurnal thermal wave the efficient heat conduction across the volume of the body makes temperature differences on the surface very small. However, *Breiter et al.* (2010a) suggested that in the same limit the YORP strength becomes $\propto 1/R$, still increasing for small objects. Additionally, their result was only concerned with the thermal component of the YORP effect, while the part related to the direct sunlight scattering in optical waveband continues to scale with $\propto 1/R^2$. Thus, the fate of the rotation of small meteoroids is still unknown at present.

The principal difference in complexity of the YORP effect results in equations (4) and (5), as compared to simple estimates in equations (1) and (2) for the Yarkovsky effect, is their infinite series nature. The nondimensional coefficients A_n and B_n in equations (4) and (5) are determined by the shape of the body, either analytically or semianalytically (e.g., *Nesvorný and Vokrouhlický,* 2007, 2008a; *Scheeres and Mirrahimi,* 2008; *Breiter and Michałska,* 2008; *Kaasalainen and Nortunen,* 2013). Interestingly, analytical methods help us to understand the torque component that changes the spin rate and the components that change the axis orientation couple, at leading order, to different attributes of the surface. The spin torque couples to chirality — the difference between eastward and westward facing slopes — while the other components couple merely to asphericity. Mathematically, this concerns the symmetric and antisymmetric terms in the Fourier expansion of the topography. If mutual shadowing of the surface facets is to be taken into account, one may use the semianalytic approach mentioned by *Breiter et al.* (2011) (see also *Scheeres and Mirrahimi,* 2008). Depending on details of the shape, the series in equations (4) and (5) may either converge quickly, with the first few terms dominating the overall behavior, or may slowly converge, with high-degree terms continuing to contribute (e.g., *Nesvorný and Vokrouhlický,* 2007, 2008a; *Kaasalainen and Nortunen,* 2013).

While this behavior had been noticed in analytical modeling, a detailed numerical study of YORP sensitivity on astronomically motivated, small-scale surface features such as craters and/or boulders was performed by *Statler* (2009). This also allowed Statler to suggest a new direction to YORP studies. He noted that the sensitivity of YORP on such small-scale features may affect its variability on short enough timescales to significantly modify the long-term evolution of the rotation rate, with the evolution changing from a smooth flow toward asymptotic state to a random walk (section 2.2).

The quadrupole (2n = 2), being the highest multipole participating in the series expansion in equations (4) and (5), is related to the assumption of coincidence between the reference frame origin and the geometric center of the body (i.e., its center of mass for homogeneous density distribution). If instead the rotation axis is displaced from this point, additional terms in the series become activated and the coefficients $(A_n;B_n)$ become modified, and thus the predicted YORP torque will change (e.g., *Nesvorný and Vokrouhlický,* 2007, 2008a). This theoretical possibility has found an interesting geophysics interpretation for (25143) Itokawa's anomalously small YORP value by *Scheeres and Gaskell* (2008) [see section 3.2, *Breiter et al.* (2009), and eventually *Lowry et al.* (2014)].

2.2. Frontiers in Modeling Efforts

2.2.1. Resolved and unresolved surface irregularities. While the models discussed above suffice to describe broad-

scale features of the Yarkovsky and YORP effects, there are important aspects that are intrinsically *nonlinear*. Current models need to explicitly treat these nonlinearities in order to capture the physical essence of radiation recoil mechanisms and to provide precise predictions. Here we discuss some recent efforts along these lines.

The simplest of such nonlinear effects is shadowing of some parts of the surface by other parts, which can occur on surfaces that are not convex. By blocking the Sun, shadowing lowers the incident flux, and increases the temperature contrast, compared to the clear-horizon case. Computationally, shadowing requires testing whether the sunward-pointing ray from each surface element intersects another surface element (e.g., *Vokrouhlický and Čapek,* 2002). This "who blocks whom" problem is of $O(N^2)$ complexity (where N is the number of surface elements); but there are strategies for storing an initial $O(N^2)$ calculation so that all subsequent calculations are only $O(N)$ (e.g., *Statler,* 2009).

Closely related to shadowing are the processes of *self-heating* (e.g., *Rozitis and Green,* 2013); these can be split conceptually into *self-illumination*, in which a surface element absorbs reflected solar flux from other parts of the surface, and *self-irradiation*, where it absorbs reradiated thermal infrared. Self-heating has the tendency to reduce the temperature contrast, by illuminating regions in shadow. Computing these effects requires prescriptions for the angular distribution of reflected and reradiated power from an arbitrary surface element, as well as the solution to the "who sees whom" problem — similar to the "who blocks whom" problem from shadowing. But since energy is traded between pairs of surface elements, self-heating, unlike shadowing, is unavoidably $O(N^2)$ if full accuracy is required.

As mentioned in section 2.1, a periodic driving at a frequency ν introduces a length scale, the thermal skin depth ℓ_ν. Asteroid surfaces are driven quasiperiodically, with the fundamental modes at the diurnal and seasonal frequencies. For typical materials, ℓ_ν is on the order of meters for the seasonal cycle and millimeters to centimeters for the diurnal cycle. If the surface's radius of curvature s satisfies the condition $s \gg \ell_\nu$, one can consider surface elements to be independent (facilitating parallelization) and solve the heat conduction problem as a function of the depth only. The radiated flux then depends on the material parameters only through the thermal inertia Γ. Most models that treat conduction explicitly do so in such one-dimensional approximation. Standard finite-difference methods are typically used to find a solution over a rotation or around a full orbit; but numerical convergence can be slow [although acceleration schemes were also considered (*Breiter et al.,* 2010b)]. Whether the condition $s \gg \ell_\nu$ is truly satisfied depends on the scale on which topography is resolved. A surface boulder can give an object a locally small radius of curvature and three-dimensional effects may become important. Full three-dimensional conduction is computationally expensive (e.g., *Golubov et al.,* 2014; *Ševeček et al.,* 2015), but the potential consequences are significant. In this case, a general finite-element method is used to solve the heat diffusion problem.

Surface roughness concerns the effects of unresolved texture on reflection, absorption, and reradiation. Parametric models for a rough-surface reflectance are well developed [e.g., see *Hapke* (1993), and references therein; and see *Breiter and Vokrouhlický* (2011) for an application to the YORP effect], although the functional forms and parameter values are matters of current research. Models for the thermal emission are at present purely numerical. In the most complete implementation (*Rozitis and Green,* 2012, 2013), a high-resolution model of a crater field is embedded inside a coarse-resolution model of a full object. The primary effects of roughness in this model are to enhance the directionality ("beaming") of the radiated intensity (relative to Lambertian emission), and to direct the radiated momentum slightly away from the surface normal, toward the Sun. Roughness models for emission and for reflection are not automatically mutually consistent, and the emission models employ the one-dimensional approximation for heat conduction despite the likelihood that s may not be much larger than ℓ_ω at the roughness scale.

Finally, nonlinear *dynamical coupling* affects both spin evolution and the orbital drift modulated by the spin state. Yarkovsky evolution models have generally incorporated heuristic prescriptions based on the YORP cycle (e.g., *Rubincam,* 2000; *Vokrouhlický and Čapek,* 2002), with possibly important effects of spin-induced material motion or reshaping included only in rudimentary ways. These processes may be modeled with particle-based discrete-element numerical codes (e.g., *Richardson et al.,* 2005; *Schwartz et al.,* 2012) and seminumerical granular dynamics in predefined potential fields (e.g., *Scheeres,* 2015). Simulated rubble piles artificially fed with angular momentum are seen to reshape and shed mass (e.g., *Walsh et al.,* 2008; *Scheeres,* 2015). Linking a particle code with a thermophysical YORP model would then allow the coupled spin and shape evolution to be followed self-consistently.

Statler (2009) argued that topographic sensitivity would make rubble piles, or any objects with loose regolith, susceptible to possibly large changes in torque triggered by small, centrifugally driven changes in shape. Repeated interruptions of the YORP cycle might then render the overall spin evolution stochastic and significantly extend the timescale of the YORP cycles (self-limitation property of YORP). *Cotto-Figueroa et al.* (2015) have tested this prediction by simulating self-consistently the coupled spin and shape evolution (toggling between configurations in a limit cycle), and stagnating behaviors that result in YORP *self-limitation. Bottke et al.* (2015) implemented a heuristic form of such stochastic YORP in a Yarkovsky drift model to find an agreement with the structure of the Eulalia asteroid family.

Accurate Yarkovsky measurements allow constraining mass and bulk density (section 4.1), but rely on precise models, with an important component due to the surface features discussed above. *Rozitis and Green* (2012) show that surface roughness can increase the Yarkovsky force by tens of percent, owing mainly to the beaming. Including the seasonal effect caused by the deeper-penetrating thermal wave can

have a comparable influence. Self-heating, in contrast, has a minimal influence on Yarkovsky forces (e.g., *Rozitis and Green,* 2013). On the other hand, the same works indicate that the YORP effect is in general dampened by beaming because it equalizes torques on opposite sides of the body.

Golubov and Krugly (2012) highlight another small-scale aspect of the YORP effect: an asymmetric heat conduction across surface features for which $s \lesssim \ell_\omega$. A rock conducts heat from its sunlit east side to its shadowed west side in the morning, and from its west side back to its east side in the afternoon. Owing to nighttime cooling, the morning temperature gradient is steeper, and hence more heat is conducted to, and radiated from, the west side, resulting in an eastward recoil. Clearly, if the collective cross section of such surface features is large, details of conduction across them may have significant consequences. Ideally, the situation calls for a complete three-dimensional heat transfer model (e.g., *Golubov et al.,* 2014; *Ševeček et al.,* 2015). Importantly, these studies indicate an overall tendency for YORP to spin objects up. However, a better understanding of small-scale surface effects is essential to understand YORP's long-term dynamics.

2.2.2. Time domain issues (tumbling). A particular problem in the modeling of the thermal effects occurs for tumbling bodies. This is because solving the heat diffusion in the body also involves the time domain. While the spatial dimensions are naturally bound, the time coordinate in general is not. However, both analytical and numerical methods involve finite time domains: The analytical approaches use a development in the Fourier series, while the effective numerical methods use iterations that require one to identify configurations at some moments in time. For bodies rotating about the principal axis of the inertia tensor, thus having a fixed direction in the inertial space, it is usually easy to modify the rotation period within its uncertainty limits such that it represents an integer fraction of the orbital period. The orbital period is then the fundamental time interval for the solution. This picture becomes more complicated for tumbling objects whose rotation is not characterized by a single time period. Rather, it is fully described with two periods, the proper rotation period and precession period, which may not be commensurable.

This situation has been numerically studied by *Vokrouhlický et al.* (2005a) in the case of (4179) Toutatis, and more recently in the case of (99942) Apophis by *Vokrouhlický et al.* (2015). Both studies suggest the tumbling may not necessarily "shut down the Yarkovsky effect," at least in the large-bodies regime. Rather, it has been found that the Yarkovsky acceleration for these tumbling objects is well represented by a simple estimate valid for bodies rotating about the shortest axis of the inertia tensor in a direction of the rotational angular momentum and with the fundamental period of tumbling, generally the precession period.

2.2.3. More than one body (binarity). Another particular case is the Yarkovsky effect for binaries (see *Vokrouhlický et al.,* 2005b). Unless the satellite has nearly the same size as the primary component, the rule of thumb is that the heliocentric motion of the system's center of mass is affected primarily by the Yarkovsky acceleration of the primary component, while the motion of the satellite feels the Yarkovsky acceleration of the satellite itself. Nevertheless, a secular change in the orbit of the satellite is actually caused by an interplay of the thermal effects and the shadow geometry in the system dubbed the Yarkovsky-Schach effect [and introduced years ago in space geodesy (*Rubincam,* 1982)]. However, it turns out that the BYORP effect, discussed in section 2.3, is more important and dominates the orbital evolution of the satellite.

2.3. Binary YORP

The binary YORP (BYORP) effect was first proposed in a paper by *Ćuk and Burns* (2005). They noted that an asymmetrically shaped synchronous secondary asteroid in a binary system should be subject to a net force differential that acts on average in a direction tangent to the orbit. Thus, as the secondary orbits about the primary body and maintains synchronicity, this would lead to either an acceleration or deceleration of the secondary, which would cause the mutual orbit of the system to spiral out or in, respectively. This seminal paper presented a basic conceptual model for the BYORP effect and provided a broad survey of many of the possible implications and observable outcomes of this effect. It also numerically studied the evolution of randomly shaped secondary bodies over a year to establish the physical validity of their model. It is key to note that a necessary condition for the BYORP effect is that at least one of the bodies be synchronous with the orbit, and it can be shut off if both bodies are nonsynchronous. Ćuk and Burns concluded that the BYORP effect should be quite strong and lead binary asteroids to either spiral in toward each other or cause them to escape in relatively short periods of time. This was further expanded in a second paper by *Ćuk* (2007) that outlined significant implications for the rate of creation and destruction of binary asteroid systems in both the near-Earth asteroid (NEA) and main-belt population, leading to the initial estimate of binary asteroid lifetimes due to BYORP on the order of only 100 k.y.

McMahon and Scheeres (2010a,b) then developed a detailed analytical model of the BYORP effect that utilized the existing shape model of the (66391) 1999 KW_4 binary asteroid satellite (*Ostro et al.,* 2006). In their approach the solar radiation force was mapped into the secondary-fixed frame and expanded as a Fourier series, following a similar approach to the YORP model development of *Scheeres* (2007). This enables any given shape model to be expressed with a series of coefficients that can be directly computed, and allows for time averaging. Using this approach they showed that the primary outcome of the BYORP effect could be reduced to a single parameter — the so-called "BYORP coefficient," B — uniquely computed from a given shape model. Henceforth, if the secondary is in a near-circular orbit, the entire BYORP effect results in simple evolutionary equations for semimajor axis a and eccentricity $e(\ll 1)$ of the binary orbit

$$\frac{da}{dt} = \frac{FB}{c\eta'} \frac{a^{3/2}}{m_2\sqrt{\mu}} \tag{6}$$

$$\frac{de}{dt} = -\frac{FB}{4c\eta'} \frac{ea^{3/2}}{m_2\sqrt{\mu}} \tag{7}$$

where again F is the solar radiation flux at the heliocentric distance a′ (equal to the semimajor axis of the heliocentric orbit), $\eta' = \sqrt{1 - e'^2}$ with e′ being the eccentricity of the heliocentric orbit, c the light velocity, m_2 the mass of the secondary, and $\mu = G(m_1 + m_2)$ the gravitational parameter of the binary system. If the orbit is expansive (B > 0), the eccentricity will be stabilized, and vice-versa (see *Ćuk and Burns,* 2005). In the case where the binary orbit is highly elliptic, the evolutionary equations become much more complex, and require additional Fourier coefficients to be included into the secular equations, as discussed in detail in *McMahon and Scheeres* (2010a).

The BYORP coefficient B is computed as a function of the shape of the body and the obliquity of the binary's orbit relative to the heliocentric orbit of the system. Assume a model for the instantaneous solar radiation force acting on the secondary has been formulated by some means, denoted as $\mathbf{F}_{SRP}(M,M')$, where M and M′ are the mean anomalies of the binary mutual orbit and heliocentric orbit, respectively. Then the computation of the BYORP coefficient requires double averaging of the radiation force over the binary and heliocentric revolution cycles, and projection in the direction of binary orbital motion (denoted here in abstract as $\hat{\mathbf{t}}$)

$$B = \hat{\mathbf{t}} \cdot \frac{1}{(2\pi)^2} \int_0^{2\pi} \int_0^{2\pi} \frac{\mathbf{F}_{SRP}}{P(r_s)} \, dM \, dM' \tag{8}$$

where $P(r_s) = (F/c)\,(a'/r_s)^2$ is the solar radiation pressure acting on the unit surface area of the body at the heliocentric distance r_s. The normalization by P implies that units of the BYORP coefficient are measured in area; thus B can be further normalized by dividing it by the effective radius squared of the secondary body. The BYORP coefficient is a function of several physical quantities such as albedo, surface topography, and potentially thermophysical effects. However, the strongest variation of the BYORP coefficient is seen to vary with the binary obliquity with respect to the heliocentric orbit (Fig. 1). If the synchronous body is rotated by 180° relative to the orbit, then the sign of the BYORP coefficient will be uniformly reversed. Due to this, when a body initially enters into a synchronous state it is supposed that the probability of it being either positive or negative is 50%.

A more recent analysis of the BYORP effect was published by *Steinberg and Sari* (2011), who found a positive correlation between the strength of the BYORP and YORP effects for bodies, and provided predictions related to the BYORP-driven evolution of the obliquity of a binary asteroid. In addition, they probed the possible effects of thermophysical models on the evolution of a binary system.

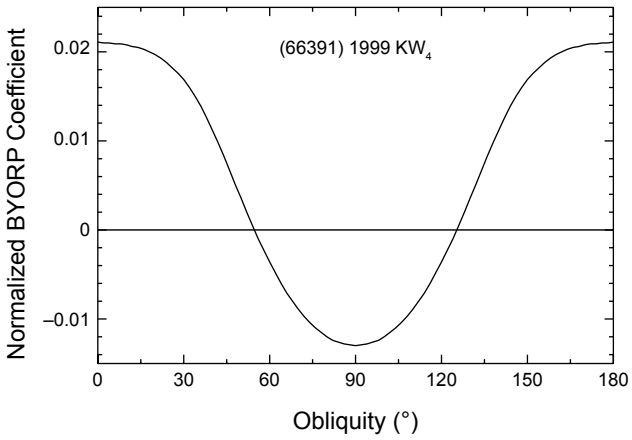

Fig. 1. BYORP coefficient B, normalized by the square of the effective radius, computed for the secondary of the (66391) 1999 KW_4 binary asteroid system, as a function of the binary orbital obliquity (abscissa).

The above discussions focus on the effect of BYORP in isolation, and not in conjunction with other evolutionary effects. However, recent work has found that the BYORP effect can mix with other evolutionary effects in surprising ways that require additional verification and study. These are primarily discussed later in section 5.3, where the long-term evolution of binary systems subject to BYORP is briefly considered. However, one of these combined effects has significant implications and is discussed here.

In particular, *Jacobson and Scheeres* (2011b) proposed the existence of an equilibrium between the BYORP effect and tides. For this equilibrium to exist, the BYORP coefficient must be negative, leading to a contractive system, and the primary asteroid must be spinning faster than the orbit rate. This creates a tidal dissipation torque that acts to expand the secondary orbit. Based on current theories of energy dissipation within rubble-pile asteroids (e.g., *Goldreich and Sari,* 2009), *Jacobson and Scheeres* (2011b) noted that all singly-synchronous rubble-pile binary asteroids with a negative BYORP coefficient for the secondary should approach a stable equilibrium that balances these two effects. This is significant, as it provides a mechanism for the persistent effect of BYORP to become stalled, leaving binary asteroids that should remain stable over long time spans. This, in turn, means that rapid formation of binary asteroids is not needed to explain the current population.

3. DIRECT DETECTIONS

Accurate observations have now allowed direct detections of both the Yarkovsky and YORP effects. This is an important validation of their underlying concepts, but also it motivates further development of the theory. These direct detections have two aspects of usefulness or application. First, the Yarkovsky effect is being currently implemented as a routine part of the orbit determination of small NEAs whose orbits are accurately constrained in the forefront software packages.

Additionally, the Yarkovsky effect is already known to be an essential part of the Earth impact hazard computations in selected cases (section 4.2 and the chapter by Farnocchia et al. in this volume). Second, many applications of the Yarkovsky and YORP effects involve statistical studies of small-body populations in the solar system rather than a detailed description of the dynamics of individual objects. Aside from a general validation, the known detections help in setting parameter intervals that could be used in these statistical studies.

3.1. Yarkovsky Effect

The possibility of detecting the Yarkovsky effect as a measurable orbital deviation was first proposed by *Vokrouhlický et al.* (2000). The idea is at first astounding given that the transverse thermal recoil force on a half-kilometer NEA should be at most 0.1 N, causing an acceleration of only ~1 pm s^{-2}. And yet such small perturbations can lead to tens of kilometers of orbital deviation for 0.5-km NEAs after only a decade. In principle, such a deviation is readily detectable during an Earth close approach, either by optical or radar observations, but the key challenge is that the precision of the position prediction must be significantly smaller than the Yarkovsky deviation that is to be measured. In practical terms, this means that detection of the Yarkovsky effect acting on a typical 0.5-km NEA requires at least three radar ranging apparitions spread over a decade, or several decades of optical astrometry in the absence of radar ranging. Of course, smaller objects could in principle reveal the Yarkovsky effect much more quickly, but the problem for small objects is that it is more difficult to build up suitable astrometric datasets. Because of this, only a few objects with diameters D < 100 m have direct detections of the Yarkovsky effect.

It should be pointed out that observations do not allow measurement of the secular change in the orbital semimajor axis directly. Rather, they reveal an associated displacement in the asteroid position along the orbit, an effect that progresses $\propto t^2$ in a given time t (see *Vokrouhlický et al.,* 2000). This is similar to the way the YORP effect is observed as discussed in section 3.2.

As predicted by *Vokrouhlický et al.* (2000), (6489) Golevka was the first asteroid with an unambiguous detection of the signature of the Yarkovsky effect in its orbit (*Chesley et al.,* 2003). In this case the detection was possible only due to the availability of three well-separated radar ranging apparitions, in 1991, 1995, and 2003. The first two radar apparitions constrain the semimajor axis, affording a precise position prediction in 2003, while the 2003 radar ranging revealed a deviation from a ballistic trajectory. Figure 2 depicts the predicted 2003 delay-Doppler observations with their uncertainty along with the associated uncertainties. The predictions were well separated with >90% confidence, and the actual asteroid position fell close to the Yarkovsky prediction.

The second reported detection of the Yarkovsky effect was for (152563) 1992 BF, which was also the first detection that did not rely on radar astrometry (*Vokrouhlický et al.,* 2008). This 0.5-km asteroid had a 13-yr optical arc (1992–2005) and four archival positions over two nights dating to 1953. These so-called precovery observations could not be fit to a purely gravitational orbit, but including the Yarkovsky effect in the orbit fitting enabled the observations to fit well and allowed a da/dt estimate with the signal-to-noise ratio SNR ≃ 15 (Fig. 3). In these cases, where the detection relies heavily on isolated and archival data, caution is warranted to avoid the possibility that mismeasurement or astrometric time tag errors are corrupting the result. As depicted in Fig. 3, the 1953 position offsets could not be attributed to timing errors, and the trail positions were remeasured with modern catalogs.

In subsequent studies a progressively increasing number of Yarkovsky detections have been announced (*Chesley et al.,* 2008; *Nugent et al.,* 2012a; *Farnocchia et al.,* 2013b). The most precise Yarkovsky measurement is that of (101955) Bennu, the target of the OSIRIS-REx asteroid sample return mission, which has a 0.5% precision Yarkovsky detection, by far the finest precision reported to date. At the extremes, asteroid 2009 BD is the smallest object (D ~ 4 m) with a verified Yarkovsky detection, which was achieved

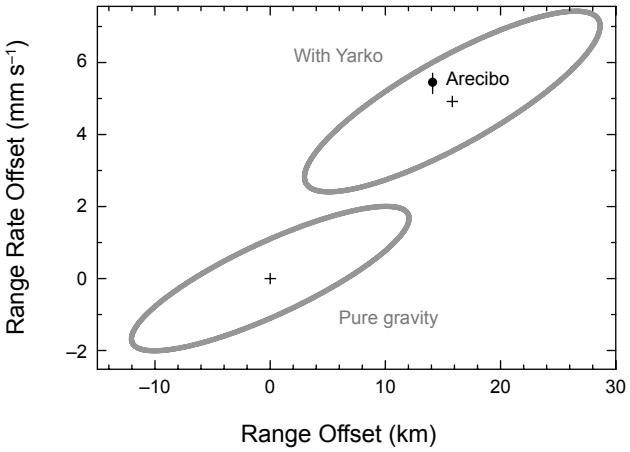

Fig. 2. Orbital solution of near-Earth asteroid (6489) Golevka from astrometric data before May 2003 projected into the plane of radar observables: (1) range at the abscissa, and (2) range-rate on the ordinate. The origin referred to the center of the nominal solution that only includes gravitational perturbations. The gray ellipse labeled "pure gravity" represents a 90% confidence level in the orbital solution due to uncertainties in astrometric observations as well as small body and planetary masses. The center of the gray ellipse labeled "with Yarko" is the predicted solution with the nominal Yarkovsky forces included (taken from *Vokrouhlický et al.,* 2000); note the range offset of ~15 km and the range rate offset of ~5 mm s^{-1}. The actual Arecibo observations from May 24, 26, and 27, 2003, are shown by the black symbol (the measurement uncertainty in range is too small to be noted in this scale). The observations fall perfectly in the uncertainty region of the orbital solution containing the Yarkovsky forces. Adapted from *Chesley et al.* (2003).

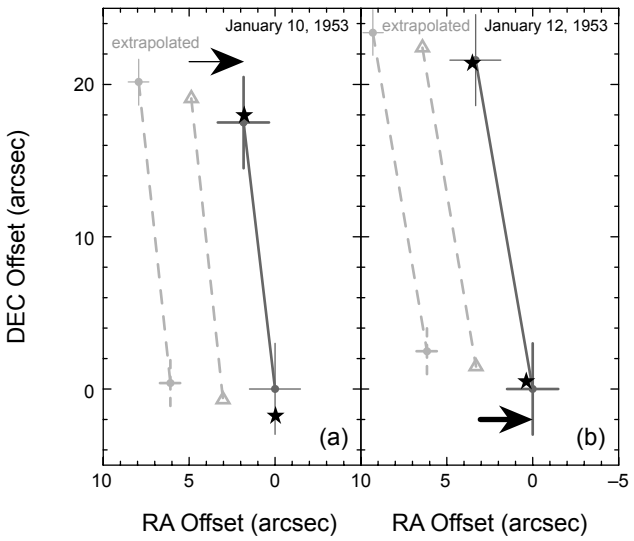

Fig. 3. Measured and predicted positions of (152563) 1992 BF on **(a)** January 10 and **(b)** January 12, 1953. The dark gray solid line is the asteroid trail appearing on Palomar plates on the two nights. Coordinate origin, right ascension at the abscissa, and declination at the ordinate are arbitrarily set to the end of the respective trail. The leftmost dashed trail labeled "extrapolated" represent pure extrapolation of the modern orbit without the thermal forces included. The mismatch in right ascension slightly improves if the 1953 data are included in the orbital solution as shown by the middle dashed trail. Still, the solution is more than 3σ away from the measured trail. Only when the thermal accelerations are included in the orbital solution do the predicted orbital positions match the observations: Stars show fitted position at the beginning and the end of the trail. Adapted from *Vokrouhlický et al.* (2008).

because of its Earth-like orbit and the 2-yr arc of observations that the orbit enabled (*Mommert et al.,* 2014). On the large end, there are two detections of 2- to 3-km-diameter asteroids, namely (2100) Ra-Shalom and (4179) Toutatis (*Nugent et al.,* 2012a; *Farnocchia et al.,* 2013b), which are both exceptionally well observed, having four and five radar apparitions, respectively.

To initially test for a signal from the Yarkovsky effect in the astrometric data of a given object, one can fit the orbit with a transverse nongravitational acceleration $a_T = A_2/r^2$, with A_2 being an estimated parameter, in addition to the orbital elements. This simple model yields a mean semimajor axis drift rate proportional to A_2, thus capturing the salient orbital deviation due to the Yarkovsky effect. The approach of using a one-parameter (A_2) Yarkovsky model is particularly convenient because it completely bypasses the thermophysical processes that are otherwise fundamental to the Yarkovsky effect. Instead, by focusing only on the level of perturbation visible in the orbit, one is able to discern the Yarkovsky effect in the absence of any knowledge of physical properties. And yet, as we shall see in section 4.1, the detection of a Yarkovsky drift can be used to estimate or infer a number of the physical and dynamical characteristics of the body. Obviously, in the case of bodies with particular interest, one can use a detailed thermophysical model of the Yarkovsky acceleration for the orbit determination in a subsequent analysis.

A population-wise, head-on approach to Yarkovsky detection thus starts with the list of asteroids with relatively secure orbits, e.g., at least 100 d of observational arc, among the NEAs. For each considered object the statistical significance of the Yarkovsky effect is obtained from the estimated value of A_2 and its *a posteriori* uncertainty σ_{A_2} according to $SNR = |A_2|/\sigma_{A_2}$, where SNR > 3 is generally considered to be a significant detection. Another parameter that is helpful in interpreting the results for a given object is the ratio between the estimated value of A_2 and the expected value for extreme obliquity and the known or inferred asteroid size, which we call $A_{2_{max}}$. The value of $A_{2_{max}}$ can be obtained by, for instance, a simple diameter scaling from the Bennu result (*Farnocchia et al.,* 2013b; *Chesley et al.,* 2014). The ratio $S = A_2/A_{2_{max}} = SNR/SNR_{max}$ provides an indication of how the estimated value of A_2 compares to what could be theoretically expected. A value of $S \gg 1$ indicates that the transverse nongravitational acceleration may be too strong to be related to the Yarkovsky effect. This could imply that the body has a far smaller density or size than assumed, or that nongravitational accelerations other than Yarkovsky are at play. A large value of S could also imply a spurious A_2 estimate due to corrupt astrometry in the orbital fit. On the other hand, $S \ll 1$ would suggest the possibility of higher density, size, or surface thermal inertia than assumed, but is often more readily explained by mid-range obliquity, which tends to null the diurnal component of the Yarkovsky drift.

Figure 4 depicts the distribution of NEAs in the SNR and SNR_{max} space that we divide into four regions:

- We consider cases with SNR > 3 and $S < 1.5$ to be *valid detections* because the estimated value is no more than 50% larger than expected, perhaps as a result of unusually low density or a size far smaller than assumed. Table 1 lists the 36 objects with valid Yarkovsky detections given currently available astrometry.
- *Spurious detections* are those with SNR > 3 and $S > 1.5$. Many of these are due to astrometric errors in isolated observation sets, such as precoveries, and can be moved to the left in Fig. 4 by deweighting the questionable data. We find 56 cases in this category, but only 12 with SNR > 4. There are two spurious cases with SNR > 10 and $S \gtrsim 10$ that cannot be due to astrometric errors and are yet unlikely to be attributed to the Yarkovsky effect.
- There are a number of objects with relatively low values for σ_{A_2} and yet the orbit does not reveal an SNR > 3 detection (denoted as *weak signal* zone on Fig. 4). Specifically, these cases have $SNR_{max} > 3$ and SNR < 3, with $S < 2/3$. These cases are potentially interesting because they generally

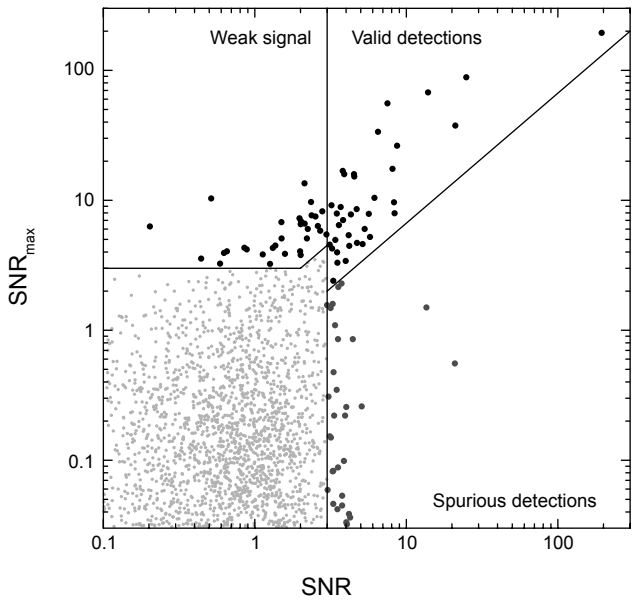

Fig. 4. SNR = A_2/σ_{A_2}, with A_2 being the parameter of an empirical transverse acceleration and σ_{A_2} its formal uncertainty, for reliable orbits of NEAs at the abscissa. The ordinate shows SNR_{max}, the maximum expected value of SNR for the body (from an estimate of its size and given an extremal obliquity, optimizing the Yarkovsky effect). Various classes of solutions, organized into four sectors by the straight lines, are discussed in the text. Situation as of December 2014.

indicate a mid-range obliquity and, despite the lack of significance in the A_2 estimate, useful bounds can be still placed on the Yarkovsky mobility of the object. We find 35 such cases in the current NEA catalog, six of which have $S < 0.05$ (Table 2). In fact, this class warrants further dedicated analysis, similar to the search of new detections.

- The vast majority of NEAs are currently uninteresting due to SNR < 3 and $SNR_{max} < 3$, meaning that no detection was found nor was one reasonably expected.

It is worth noting that objects with nonprincipal-axis rotation states can reveal the Yarkovsky effect (e.g., *Vokrouhlický et al.,* 2005a); (4179) Toutatis is a large, slowly tumbling asteroid (e.g., *Hudson and Ostro,* 1995) with Yarkovsky SNR ≃ 8 (and $S \simeq 1$) due to an extensive set of radar ranging data. Also, the much smaller asteroid (99942) Apophis, which has been reported to have a measurable polar precession (*Pravec et al.,* 2014), presently has a solid Yarkovsky signal with SNR ≃ 1.8 (and $S < 1$), although not high enough to be listed in Table 1, but still significant in light of the abundant radar astrometry available for Apophis (*Vokrouhlický et al.,* 2015). Similarly, binary asteroid systems may also reveal Yarkovsky drift in their heliocentric orbits (e.g., *Vokrouhlický et al.,* 2005b), although none presently appears in Table 1. We note that (363599) 2004 FG_{11} has a satellite (*Taylor et al.,* 2012) and currently has a Yarkovsky SNR ≃ 2.8 (and $S \simeq 1$).

3.2. YORP Effect

Analyses of small-asteroid populations indicate clear traits of their evolution due to the YORP effect, both in rotation rate and obliquity (sections 4.5, 5.1, and 5.2). Accurate observations of individual objects, however, do not presently permit detection of the secular change in obliquity and reveal only the secular effect in rotation rate. Even that is a challenging task, because the YORP torque has a weak effect on kilometer-sized asteroids at roughly 1 AU heliocentric distance. Similar to the case of the Yarkovsky effect, the YORP detection is enabled via accurate measurement of a phase ϕ associated with the rotation rate. This is because when the rotation frequency ω changes linearly with time, $\omega(t) = \omega_0 + (d\omega/dt)\,t$ (adopting the simplest possible assumption, since $d\omega/dt$ may have its own time variability), the related phase ϕ grows quadratically in time, $\phi(t) = \phi_0 + \omega_0 t + \frac{1}{2}(d\omega/dt)\,t^2$. Additionally, other perturbations (such as an unresolved weak tumbling) do not produce an aliasing signal that would disqualify YORP detection. So the determination of the YORP-induced change in the rotation rate $d\omega/dt$ may basically alias with the rotation rate frequency ω_0 itself in the $d\omega/dt = 0$ model. This is because small variations in ω_0 propagate linearly in time in the rotation phase. The YORP detection stems from the ability to discern this linear trend due to the ω_0 optimization and the quadratic signal due to a nonzero $d\omega/dt$ value. In an ideal situation of observations sufficiently densely and evenly distributed over a given time interval T, one avoids the ω_0 and $d\omega/dt$ correlation setting time origin at the center of the interval. At the interval limits the YORP effect manifests via phase change $\simeq\frac{1}{8}(d\omega/dt)T^2$. Therefore, a useful approximate rule is that the YORP effect is detected when this value is larger than the phase uncertainty $\delta\phi$ in the observations. Assuming optimistically $\delta\phi \simeq 5°$ and T about a decade, the limiting detectable $d\omega/dt$ value is $\simeq 5 \times 10^{-8}$ rad d^{-2}. Obviously, detection favors a longer time-base T if accuracy of the early observations permits. In practice, the late 1960s or early 1970s was the time during which photoelectric photometry was introduced and allowed sufficiently reliable light curve observations. This sets a maximum T of about 40 yr today for bright-enough objects [e.g., (1620) Geographos (*Ďurech et al.,* 2008a); see, for completeness, an interesting YORP study for asteroid (433) Eros by *Ďurech* (2005)]. We should also mention that ω and ϕ above denote sidereal rotation rate and phase, respectively. Hence to convert asteroid photometry to ϕ one needs to know the orientation of its spin axis in the inertial space and the shape model. Their solution may increase the realistic uncertainty in $d\omega/dt$ if compared to the simple estimate discussed above.

Figure 5 shows an example of detected quadratic advance in sidereal rotation phase ϕ in the case of the small coorbital asteroid (54509) YORP (see *Lowry et al.,* 2007; *Taylor et al.,* 2007). The expected YORP value of rotation-rate change matched the observed value, thus allowing interpretation of the signal as a YORP effect detection, although an accurate comparison is prohibited by lack of knowledge of

TABLE 1. List of the Yarkovsky effect detections as of December 2014.

Object	$\bar{r}$ (AU)	H (mag)	D (m)	da/dt ($\times 10^{-4}$ AU m.y.$^{-1}$)	SNR	S	Data Arc	N_{rad}
(101955) Bennu	1.10	20.6	493	–18.95 ± 0.10	194.6	1.0	1999–2013	3
(2340) Hathor	0.75	20.2	210	–17.38 ± 0.70	24.9	0.3	1976–2014	1
(152563) 1992 BF	0.87	19.7	510	–11.82 ± 0.56	21.0	0.6	1953–2011	0
2009 BD	1.01	28.2	4	–489 ± 35	13.9	0.2	2009–2011	0
2005 ES_{70}	0.70	23.7	61	–68.9 ± 7.9	8.7	0.3	2005–2013	0
(4179) Toutatis	1.96	15.1	2800	–3.75 ± 0.45	8.4	1.1	1934–2014	5
(2062) Aten	0.95	17.1	1300	–6.60 ± 0.80	8.3	0.9	1955–2014	4
1999 MN	0.50	21.4	175	54.6 ± 6.8	8.1	0.5	1999–2014	0
(6489) Golevka	2.01	19.1	280	–4.52 ± 0.60	7.5	0.1	1991–2011	3
(1862) Apollo	1.22	16.3	1400	–1.58 ± 0.24	6.5	0.2	1930–2014	2
2006 CT	1.07	22.3	119	–47.6 ± 7.7	6.2	0.6	1991–2014	1
(3908) Nyx	1.71	17.3	1000	9.6 ± 1.7	5.8	1.1	1980–2014	2
2000 PN_8	1.22	22.1	130	49.3 ± 8.7	5.7	0.7	2000–2014	0
(162004) 1991 VE	0.67	18.1	827	19.2 ± 3.6	5.3	0.9	1954–2014	0
(10302) 1989 ML	1.26	19.4	248	38.7 ± 7.5	5.2	1.1	1989–2012	0
(2100) Ra-Shalom	0.75	16.1	2240	–5.8 ± 1.2	4.7	1.0	1975–2013	4
(29075) 1950 DA	1.46	17.1	1300	–2.70 ± 0.57	4.7	0.6	1950–2014	2
(85953) 1999 FK_{21}	0.53	18.0	590	–11.0 ± 2.4	4.5	0.3	1971–2014	0
(363505) 2003 UC_{20}	0.74	18.2	765	–4.5 ± 1.0	4.5	0.3	1954–2014	1
2004 KH_{17}	0.62	21.9	197	–42.0 ± 9.8	4.3	0.6	2004–2013	1
(66400) 1999 LT_7	0.70	19.4	411	–35.0 ± 8.3	4.2	0.9	1987–2014	0
1995 CR	0.45	21.7	100	–314 ± 76	4.2	0.8	1995–2014	0
(4034) Vishnu	0.95	18.3	420	–31.8 ± 8.0	4.0	1.2	1986–2014	1
(85774) 1998 UT_{18}	1.33	19.1	900	–2.45 ± 0.63	3.9	0.2	1989–2014	3
1994 XL_1	0.57	20.8	231	–37.6 ± 9.8	3.8	0.5	1994–2011	0
(3361) Orpheus	1.14	19.0	348	6.2 ± 1.7	3.8	0.2	1982–2014	0
(377097) 2002 WQ_4	1.63	19.5	422	–9.6 ± 2.6	3.7	0.4	1950–2014	0
(138852) 2000 WN_{10}	0.97	20.1	328	17.7 ± 4.9	3.6	0.6	2000–2014	0
(399308) 1999 GD	1.07	20.8	180	47 ± 13	3.5	0.9	1993–2014	0
(4581) Asclepius	0.96	20.7	242	–19.7 ± 5.7	3.5	0.4	1989–2014	1
2007 TF_{68}	1.36	22.7	100	–60 ± 18	3.4	0.7	2002–2012	0
1999 FA	1.07	20.6	300	–43 ± 13	3.3	1.4	1978–2008	0
(2063) Bacchus	1.01	17.2	1200	–6.6 ± 2.0	3.2	0.8	1977–2014	2
(350462) 1998 KG_3	1.15	22.2	125	–25.2 ± 7.9	3.2	0.4	1998–2013	0
(256004) 2006 UP	1.51	23.0	85	–67 ± 21	3.1	0.7	2002–2014	0
(37655) Illapa	0.97	17.8	950	–10.3 ± 3.5	3.0	0.5	1994–2013	2

Reliable detections with SNR larger than 3 are listed: $\bar{r} = a\sqrt{1-e^2}$ is the solar flux-weighted mean heliocentric distance, H is the absolute magnitude, D is the diameter derived from the literature when available [and obtained here from the European Asteroid Research Node (EARN) Near-Earth Asteroids Database, *http://earn.dlr.de/nea*] or from absolute magnitude with 15.4% albedo, the da/dt and formal uncertainty $\sigma_{da/dt}$ are derived from the orbital fit (via A_2 and σ_{A_2} values as described in *Farnocchia et al.,* 2013b). SNR = $(da/dt)/\sigma_{da/dt}$ is the quality of the semimajor axis drift determination, and S = SNR/SNR_{max}, where SNR_{max} is the maximum estimated SNR for the Yarkovsky effect. Data arc indicates the time interval over which the astrometric information is available, and N_{rad} denotes the number of radar apparitions in the fit.

TABLE 2. List of the most notable Yarkovsky effect nondetections as of December 2014.

Object	$\bar{r}$ (AU)	H (mag)	D (m)	$1/S$	Data Arc	N_{rad}
(3757) Anagolay	1.65	19.1	390	86.8	1982–2014	1
(247517) 2002 QY_6	0.62	19.6	270	56.9	2002–2014	0
(5797) Bivoj	1.71	18.8	500	53.6	1953–2014	0
(152742) 1998 XE_{12}	0.62	18.9	413	39.7	1995–2014	0
(1221) Amor	1.74	17.4	1100	31.0	1932–2012	0
(225312) 1996 XB_{27}	1.19	21.7	85	20.1	1996–2014	0

Notable nondetections of the Yarkovsky effect with $1/S > 10$ are listed. Columns as in Table 1.

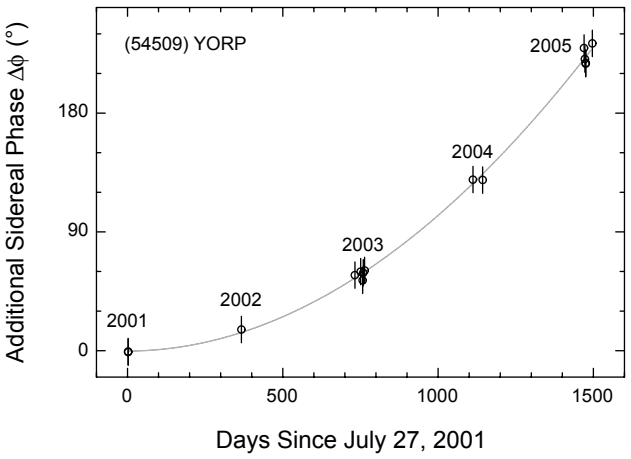

Fig. 5. Advance of the sidereal rotation phase Δϕ (ordinate in degrees) vs. time (in days) for the small Earth-coorbital asteroid (54509) YORP. Symbols are measurements with their estimated uncertainty, as follow from assembling the radar observations at different apparitions. The gray line is a quadratic progression $\Delta\phi = \frac{1}{2}(d\omega/dt)t^2$, with $d\omega/dt = 350 \times 10^{-8}$ rad d^{-2}. Time origin set arbitrarily to July 27, 2001, corresponding to the first measurement. Adapted from *Taylor et al.* (2007).

the full shape of this body (due to repeated similar viewing geometry from Earth). A complete list of the YORP detections, as of September 2014, is given in Table 3. To appreciate their accuracy, we note that they correspond to a tiny change in sidereal rotation period by a few milliseconds per year: 1.25 ms y^{-1} for (54509) YORP to a maximum value of 45 ms y^{-1} for (25143) Itokawa. While not numerous at the moment, we expect the list will more than double during the next decade. There are presently two asteroids, (1620) Geographos and (1862) Apollo, for which both Yarkovsky and YORP effects have been detected. These cases are of special value, provided a sufficiently accurate physical model of the body is available (see *Rozitis et al.,* 2013; *Rozitis and Green,* 2014).

(25143) Itokawa holds a special place among the asteroids for which the YORP effect has been detected. Not only was this the first asteroid for which YORP detection was predicted (*Vokrouhlický et al.,* 2004), but the shape of this body is known very accurately thanks to the visit of the Hayabusa spacecraft. This has led researchers to push the attempts for an accurate YORP prediction to an extreme level (e.g., *Scheeres et al.,* 2007; *Breiter et al.,* 2009; *Lowry et al.,* 2014), realizing that the results depend in this case very sensitively on the small-scale irregularities of the shape (see *Statler,* 2009, for a general concept). However, in spite of an uncertainty in the YORP prediction, the most detailed computation consistently predicted deceleration of the rotation rate by YORP, as opposed to the detected value (Table 3). A solution to this conundrum has been suggested by *Scheeres et al.* (2007), who proposed that the difference in density between the "head" and "body" of this asteroid may significantly shift the center of mass. This effect introduces an extra torque component that could overrun the YORP torque, canonically computed for homogeneous bodies, and make the predicted deceleration become acceleration of the rotation rate. *Lowry et al.* (2014) adopted this solution, predicting that the two parts of Itokawa have a very different densities of ≃1.75 g cm^{-3} and ≃2.85 g cm^{-3}. Nevertheless, the situation may be even more complicated: *Golubov and Krugly* (2012) have shown that transverse heat communication across boulder-scale features on the surface of asteroids may cause a systematic trend toward acceleration of the rotation rate. Indeed, in the most complete works so far, *Golubov et al.* (2014) and *Ševeček et al.* (2015) show that the detected acceleration of Itokawa's rotation rate may be in large part due to detailed modeling of the effects described by *Golubov and Krugly* (2012) without invoking a large density difference in the asteroid. The complicated case of Itokawa thus keeps motivating detailed modeling efforts of the YORP effect. Luckily, not all asteroidal shapes show such an extreme sensitivity on the small-scale surface features (e.g., *Kaasalainen and Nortunen,* 2013), thus allowing an easier comparison between the detected and predicted YORP signals.

On a more general level, we note that in spite of rotation periods ranging from a fraction of an hour to more than 12 h, all five asteroids for which the YORP effect was detected reveal acceleration of the rotation rate. It is not yet known

TABLE 3. List of the YORP effect detections as of September 2014.

Object		dω/dt (×10^{-8} rad/d^2)	H (mag)	P (h)	γ (deg)	$\bar{r}$ (AU)	Reference
(54509)	YORP	350 ± 35	22.6	0.203	173	0.98	*Lowry et al.* (2007); *Taylor et al.* (2007)
(25143)	Itokawa	3.5 ± 0.4	18.9	12.132	178	1.27	*Lowry et al.* (2014)
(1620)	Geographos	1.2 ± 0.2	15.6	5.223	152	1.18	*Ďurech et al.* (2008a)
(1862)	Apollo	5.5 ± 1.2	16.3	3.065	162	1.22	*Kaasalainen et al.* (2007); *Ďurech et al.* (2008b)
(3103)	Eger	1.4 ± 0.6	15.3	5.710	176	1.32	*Ďurech et al.* (2012)
(1865)	Cerberus	<0.8	16.8	6.803	178	0.96	*Ďurech et al.* (2012)

For each of the asteroids with the YORP effect detected we give (1) rotation rate change dω/dt derived from the photometric data, (2) absolute magnitude H, (3) rotation period P, (4) obliquity γ, and (5) the solar flux weighted mean heliocentric distance $\bar{r} = a\sqrt{1-e^2}$, with semimajor axis a and eccentricity e. In the case of (1865) Cerberus, the observational limit $|d\omega/dt| < 0.8 \times 10^{-8}$ rad/d^2 is nontrivial for a body of its size, orbit, and rotation state. Less severe limits on |dω/dt| were also derived for (2100) Ra-Shalom (*Ďurech et al.,* 2012) and (433) Eros (*Ďurech,* 2005).

whether this expresses observational bias against detection of the YORP-induced deceleration of the rotation rate, or whether it points toward the true asymmetry in YORP's ability to accelerate vs. decelerate rotation rate. Note that one would statistically expect to detect YORP deceleration of the rotation rate principally among asteroids rotating slowly, but this is exactly where accurate photometric observations are especially difficult. Efforts with the goal of detecting the YORP effect for asteroids with rotation periods in the 20–40-h range are underway, with the results expected in the next couple of years. Hopefully, they will help in settling the issue of possible asymmetry in the YORP effect on ω.

3.3. Binary YORP Effect

The BYORP effect has not been directly observed as of yet, although some predictions stemming from this effect have been confirmed. There are currently significant campaigns observing binary asteroids to search for predicted outcomes of the BYORP effect, both in isolation or mixing with other evolutionary effects. The basic technique for detecting the BYORP effect as it acts in solitude was proposed by *McMahon and Scheeres* (2010b) and suggests that computing the drift in a binary system's mean anomaly due to changes in the semimajor axis is the most effective approach, as this drift will increase quadratically in time as compared to purely Keplerian motion. The relative change ΔM in the mean anomaly M of a binary asteroid due to the BYORP effect in time t is $a\Delta M = -\frac{3}{4}n(da/dt)t^2$, where n is the binary mean motion and (da/dt) should be substituted from equation (6). The corresponding delay, or advance, in occultation timing of the binary is $\simeq -\frac{3}{4}[(da/dt)/a]t^2$.

McMahon and Scheeres (2010b) provide a table of known and possibly synchronous binary asteroids along with an estimate of mean anomaly drift, based on scaling the computed (66391) 1999 KW_4 BYORP coefficient to the different asteroid systems, accounting for secondary size, system mass, and heliocentric orbit. As these stated drifts make a strong assumption in applying the KW_4 BYORP coefficient, they are not true predictions, but rather provide a prediction of relative strength of the BYORP effect for different bodies. Petr Pravec has expanded this list of predicted drift rates, making them accessible in the Binary Asteroid Database (*http://www.asu.cas.cz/~asteroid/binastdata.htm*) and indicating which should have the largest, and hence easiest to detect, drifts along with other information of use to observers.

This list represents an active longer-term campaign by Pravec and colleagues to observe binary asteroid systems during predicted occultation events. The most significant result of this effort to date has been focused on the binary asteroid (175706) 1996 FG_3 (*Scheirich et al.,* 2015). For this body, observations over a 17-yr time span provided a strong "zero" constraint on the BYORP drift rate. While not a direct detection of the BYORP effect, this is fully consistent with a current prediction that involves the BYORP-tide equilibrium state. The confirmation of a binary system in this state has scientific implications as it means that the tidal dissipation that occurs within a rapidly spinning primary body can be determined once the BYORP coefficient for a secondary asteroid is determined. Although it cannot be directly measured when this will occur in such an equilibrium, it is possible to estimate the BYORP coefficient based on detailed models of the secondary and its albedo, such as could be obtained by an *in situ* spacecraft. Thus, a space mission to a binary in such a state could provide an unprecedented view into the internal geophysics of a rubble pile.

Other bodies of current interest include any binary systems with a synchronous secondary. A direct detection of BYORP is feasible if the body is in an expansive state, although the relatively short lifetime predicted for such binaries would imply that finding such a binary may be difficult. Similarly, this is also true of a contractive state, as this should be heading toward a BYORP-tide equilibrium. Additional measurements are important, however, as the number of binaries found to be in the equilibrium state relative to the number found in expansive or contractive states will be an important measurement with implications beyond the BYORP effect in isolation. Specifically, such observations could provide insights into the internal tidal dissipation of energy that occurs for rubble-pile binary asteroid primaries (e.g., *Jacobson and Scheeres,* 2011b).

4. APPLICATIONS OF THE YARKOVSKY EFFECT

4.1. Physical Properties of Asteroids

The Yarkovsky effect can be used as a tool to probe the nature of individual asteroids. This is possible because an asteroid's Yarkovsky drift is a manifestation of several of its physical properties, and so a direct measurement of da/dt allows insight into the characteristics of the body. Of primary importance are the obliquity, size, and mass of the asteroid, although the thermal and reflective properties and the rotation rate are also important.

Not surprisingly, the more that is known about the asteroid, the more that can be divined from a Yarkovsky detection. In the weakest situation, which is not so unusual, we have only da/dt and the absolute magnitude H. Even in this case we can already put meaningful constraints on the obliquity of the body through the cos γ dependence. For instance, the sign of da/dt reveals immediately whether the rotation is retrograde or direct. Moreover, the value of *S* from Table 1 can serve as a proxy for |cos γ|, while variations in ρD and Θ_ω add uncertainty to this estimate. *Vokrouhlický et al.* (2008) used this principle to infer that (152563) 1992 BF must have obliquity $\gamma > 120°$, after accounting for reasonable variations in other unknowns.

If the spin state of the body is known, generally from some combination of radar imaging and optical light curves, we have a much clearer insight into the nature of the body because cos γ is removed as an unknown and the thermal parameter Θ_ω is better constrained. Indeed, in such cases we are left with a simple relationship between ρD and the

thermal inertia Γ. But the diameter D can be measured directly by radar, or inferred from taxonomic type or measured albedo, or can just be derived from an assumed distribution of asteroid albedo, allowing the constraint to be cast in terms of the bulk density ρ and thermal inertia Γ. The gray region of Fig. 6 depicts this type of constraint for the case of (101955) Bennu. The peak in ρ seen in Fig. 6 is associated with $\Theta_\omega \simeq 1$, where the Yarkovsky effect obtains its maximum effectiveness. This characteristic peak in the ρ vs. Γ relationship often allows strict upper bounds on ρ (e.g., *Chesley et al.,* 2003).

We note that the degeneracy between ρ and Γ could in principle be broken by an independent estimate of ρ that would allow a direct estimate of Γ, albeit with the possibility of two solutions. While this approach has so far not been possible, we anticipate it here as a natural outcome of the first detection of the Yarkovsky effect on a well-observed binary system.

Another approach to breaking the correlation between ρ and Γ makes use of measurable solar radiation pressure deviations on the orbit, which yields an area-to-mass ratio. With a size estimate, an independent mass estimate can lead to a double solution for the thermal inertia of the body (e.g., *Mommert et al.,* 2014).

The alternative approach has been applied successfully in a few special cases to date. Specifically, observations of an asteroid's thermal emissions can afford independent constraints on the thermal inertia, breaking the degeneracy between ρ and Γ, allowing a direct estimate of the asteroid's bulk density. Perhaps the most striking example here is the case of (101955) Bennu, which has a well-constrained shape, spin state, and thermal inertia. When these are linked with the high precision da/dt estimate (Table 1), the result is a bulk density of 1260 ± 70 kg m^{-3} (Fig. 6), where the formal precision is better than 6% (*Chesley et al.,* 2014). Other similar cases include (1862) Apollo, (1620) Geographos, and (29075) 1950 DA (respectively, *Rozitis et al.,* 2013, 2014; *Rozitis and Green,* 2014). In each of these cases the authors combine da/dt, radar imaging, and thermal measurements to derive the bulk density of the asteroid.

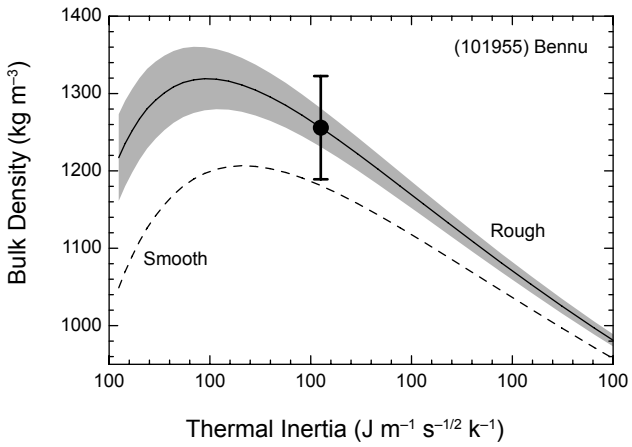

Fig. 6. Bulk density ρ solution for (101955) Bennu from detected value of the Yarkovsky orbital effect as a function of the surface thermal inertia Γ. The dashed line corresponds to the da/dt = const. solution for a smooth-surface model, taking into account a detailed shape model and a nonlinear boundary condition. The solid line accounts for 50% small-scale roughness in each of the surface facets of the shape model, while the gray zone takes into account the estimated ~17% uncertainty in the roughness value. The nonlinearity of the da/dt isoline in the ρ vs. Γ plane follows from equations (1) and (3). Adapted from *Chesley et al.* (2014).

In the best cases of Yarkovky detection, where we also have a shape model, spin state, and thermophysical characterization, one can infer the local gravity of the body. This can be of profound engineering interest for the asteroid targets of space missions, e.g., (101955) Bennu. The mission design challenges for the OSIRIS-REx mission are significantly eased due to the Yarkovsky constraint on Bennu's mass and bulk density. Another such case is (29075) 1950 DA, which is not a space mission target, and yet the estimates of local surface gravity derived from Yarkovsky have profound implications. *Rozitis et al.* (2014) found that their thermal measurements, when combined with the Yarkovsky drift reported for 1950 DA by *Farnocchia and Chesley* (2014), required a low asteroid mass. The estimated mass was so low, in fact, that it implied that the equatorial surface material on 1950 DA is in tension due to centrifugal forces. And yet the estimated thermal inertia was low enough that it required a loose, fine-grained regolith on the surface. This seeming contradiction is most readily resolved by the action of cohesive forces due to van der Waals attraction between regolith grains, and represents the first confirmation of such forces acting on an asteroid, which had already been anticipated by *Scheeres et al.* (2010). And so, through a curious interdisciplinary pathway, the measurement of the Yarkovsky drift on 1950 DA reveals the nature of minute attractive forces at work in the asteroid's regolith.

Population implications — The discussion above treats Yarkovsky detections in a case-by-case manner, deriving additional information for the specific asteroid at hand. However, the wealth of Yarkovsky detections listed in Table 1 allows an insight into the NEA population as a whole. Of particular interest is the distribution of obliquities implied by the tabulated detections, of which 28 out of 36 detections reveal da/dt < 0 and thus about 78% of the sample requires retrograde rotation (see also Fig. 9).

This excess of retrograde rotators represents an independent confirmation of a result first reported by *La Spina et al.* (2004). The mechanism for an excess of retrograde rotators in the NEA population is a result of the Yarkovsky driven transport mechanism (e.g., *Morbidelli and Vokrouhlický,* 2003). The location of the ν_6 resonance at the inner edge of the main belt implies that main-belt asteroids entering the inner solar system through this pathway must have da/dt < 0 and thus retrograde rotation. Direct rotators will tend to drift away from the resonance. Asteroids entering the inner solar system through other resonance pathways, principally the 3:1 mean-motion resonance with Jupiter, may drift either in or out into the resonance, and so will have parity between retrograde

and direct rotators. *Farnocchia et al.* (2013b) analyze this retrograde prevalence, including selection effects among the Yarkovsky detections, and find that it is fully consistent with the Yarkovsky-driven transport, and point out that this can be used to derive a distribution of the obliquities of NEAs.

4.2. Impact Hazard Assessment

Most reported potential impacts are associated with newly discovered objects for which the uncertainty at the threatening Earth encounter is dominated by the uncertainties in the available astrometric observations. However, as the astrometric dataset grows, the fidelity of the force model used to propagate the asteroid from discovery to potential impact becomes more and more important. For a few asteroids with extraordinarily precise orbits, the Yarkovsky effect is a crucial aspect of an analysis of the risk posed by potential impacts on Earth. When the Yarkovsky effect is directly revealed by the astrometric data, the analysis approach is straightforward, as is the case for (101955) Bennu and (29075) 1950 DA (e.g., *Milani et al.,* 2009; *Chesley et al.,* 2014; *Farnocchia and Chesley,* 2014).

However, there are some cases in which the astrometry provides little or no constraint on the Yarkovsky effect, and yet Yarkovsky drift is a major contributor to uncertainties at a potentially threatening Earth encounter. In these situations we are forced to assume distributions on albedo, obliquity, thermal inertia, etc., and from these we can derive a distribution of A_2 or da/dt. A Monte Carlo approach with these distributions allows us to better represent uncertainties at the threatening Earth encounter, and thereby compute more realistic impact probabilities. This technique has been necessary for (99942) Apophis and has been applied by *Farnocchia et al.* (2013a) before *Vokrouhlický et al.* (2015) made use of rotation-state determination of this asteroid. See the chapter by Farnocchia et al. in this volume) for a more complete discussion of Yarkovsky-driven impact hazard analyses.

4.3. Meteorite Transport Issues

The Yarkovsky effect, with its ability to secularly change the semimajor axes of meteoroids (precursors of meteorites, which are believed to be fragments of larger asteroids located in the main belt between the orbits of Mars and Jupiter), was originally proposed to be the main element driving meteorites to Earth (see *Öpik,* 1951; *Peterson,* 1976). However, direct transport from the main belt, say as a small body slowly spiraling inward toward the Sun by the Yarkovsky effect, required very long timescales and unrealistic values of the thermal parameters and/or rotation rates for meter-sized bodies. Moreover, a.m./p.m. fall statistics and measured preatmospheric trajectories in rare cases (like the Příbram meteorite) indicated many meteorites had orbits with the semimajor axis still close to the main-belt values.

The problem was overcome in the late 1970s and early 1980s by advances in our understanding of asteroid dynamics. Numerous works have shown that the transport routes that connect main-belt objects to planet-crossing orbits are in fact secular and mean-motion resonances with giant planets, such as the ν_6 secular resonance at the lower border of the main asteroid belt and/or the 3:1 mean-motion resonance with Jupiter. Putting this information together with the Yarkovsky effect, *Vokrouhlický and Farinella* (2000) were able to construct a model in which meteoroids or their immediate precursor objects are collisionally born in the inner and/or central parts of the main belt, from where they are transported to the resonances by the Yarkovsky effect. En route, some of the precursors may fragment, which can produce new swarms of daughter meteoroids that eventually reach the escape routes to planet-crossing orbits. With this model, Vokrouhlický and Farinella could explain the distribution of the cosmic-ray exposure ages of stony meteorites as a combination of several timescales: (1) the time it takes for a meteoroid to collisionally break, (2) the time it takes a meteoroid to travel to a resonance, (3) the time it takes for that resonance to deliver the meteoroid to an Earth-crossing orbit, and (4) the time it takes the meteoroid on a planet-crossing orbit to hit Earth.

While successful to the first order, this model certainly contains a number of assumptions and potentially weak elements, especially in the light of subsequent rapid development of the YORP effect theory, that warrant further work. For instance, one of the difficulties in refining the meteorite delivery models is the uncertainty in identification of the ultimate parent asteroid (or asteroids) for a given meteorite class (e.g., see the chapter by Vernazza et al. in this volume). Thus, among the ordinary chondrites we have a reasonable guess that LL-chondrites originate from the Flora region [or the asteroid (8) Flora itself] and the L-chondrites originate from disruption of the Gefion family. There were numerous guesses for the H-chondrite source region [such as the asteroid (6) Hebe], but none of them has been unambiguously confirmed. The model presented by *Nesvorný et al.* (2009), while more educated in the choice of the L-chondrite source region than the previous work of *Vokrouhlický and Farinella* (2000), requires immediate parent bodies of these meteorites, 5–50 m in size, to reach the powerful 3:1 mean-motion resonance with Jupiter. This means they should have migrated by the Yarkovsky effect some 0.25–0.3 AU from their source location in less than 0.5 b.y. While this is not a problem in a scenario where the bodies rotate about the body-fixed axis whose direction is preserved in the inertial space, it is not clear if this holds when the bodies would start to tumble or their axes started to evolve rapidly due to the YORP effect. Clearly, more work is needed to understand the Yarkovsky effect in the small-size limit for bodies whose spin axis may undergo fast evolution.

4.4. Orbital Convergence in Asteroid Families and Pairs

Over the past decade the Yarkovsky and YORP effects have helped to significantly boost our knowledge of the asteroid families (e.g., see the chapter by Nesvorný et al. in

this volume). This is because they represent a unique time-dependent process in modeling their structure, thus allowing us to constrain their ages for the first time.

The most accurate results are obtained for young-enough families (ages <10 m.y., say), for which effects of the deterministic chaos are weak. As shown in the pioneering works of *Nesvorný et al.* (2002, 2003), the basic tool to determine the origin of the family is provided by the convergence of orbital secular angles (the nodal and pericenter longitudes Ω and ϖ) at some moment in the past. Because the rate at which these angles precess in space depends sensitively on the semimajor axis value, the past values of Ω and ϖ of the family members depend on their Yarkovsky drift-rates da/dt. This contribution may not be negligible, because the changes in precession rates produce effects that grow quadratically in time (the same way as described in sections 3.1 and 3.2 for longitude in orbit or sidereal rotation phase). Thus *Nesvorný and Bottke* (2004) were able to significantly improve the uncertainty in the age of the Karin family by including the Yarkovsky effect in their model. At the same time, this work provided an effective detection of the Yarkovsky effect for the main-belt asteroids. This technique has been later used for age constraints of several other young families (e.g., *Novaković,* 2010; *Novaković et al.,* 2012, 2014), including sub-million-year-old clusters (e.g., *Nesvorný et al.,* 2006, 2008; *Nesvorný and Vokrouhlický,* 2006; *Vokrouhlický et al.,* 2009).

While the methods of dating young asteroid families involve convergence of the orbital angles only, the determination of ages of the asteroid pairs (e.g., *Vokrouhlický and Nesvorný,* 2008; *Pravec et al.,* 2010) represents an even more ambitious task. In this case, one seeks to achieve a full convergence of two asteroidal orbits into a single location in the Cartesian space (within the distance of about a radius of the Hill sphere of the parent body) and with a small relative velocity (comparable to the escape velocity from the parent body). It is not surprising that the Yarkovsky effect again plays important role in this effort. The best cases, such as the pair (6070) Rheinland and (54827) 2001 NQ_8, allow one to also infer constraints on the obliquities of the individual components, consequently providing predictions directly testable by further observations (e.g., *Vokrouhlický and Nesvorný,* 2009; *Vokrouhlický et al.,* 2011).

4.5. Spreading of Asteroid Families

Older asteroid families (ages >10 m.y., say) do not permit application of the fine age-determination methods described in section 4.4. This is because orbits in the main asteroid belt are affected by deterministic chaos over long timescales. Hence it is not possible to reliably reconstruct past values of the orbital secular angles, with the proper values of semimajor axis a_p, eccentricity e_p, and inclination i_p being the only well-defined parameters at hand. Still, these proper elements are constructed using approximate dynamical models, spanning time intervals quite shorter than the typical ages of large asteroid families. While the deterministic chaos is still in action over long timescales and produces a slow diffusion of the proper e_p and i_p values, the Yarkovsky effect is the principal phenomenon that changes the proper a_p values of multi-kilometer-sized asteroids. *Bottke et al.* (2001), studying an anomalous structure of the Koronis family, presented the first clear example of the Yarkovsky effect sculpting a large-scale shape of an asteroid family in a_p and e_p. It also approximately constrained its age to ~2.5–3 b.y. [see also *Vokrouhlický et al.* (2010) for a similar study of the Sylvia family].

A novel method suitable for age determination of families a few hundred million years old has been presented by *Vokrouhlický et al.* (2006a). It stems from the observation that small asteroids in some families are pushed toward extreme values of the semimajor axis and, if plotted in the a_p vs. H (absolute magnitude) diagram, they acquire an "eared" structure (Fig. 7). Since this peculiar structure is not compatible with a direct emplacement by any reasonable ejection field, *Vokrouhlický et al.* (2006a) argued it must result from a long-term dynamical evolution of the family. In particular, postulating that the initial dispersal in a_p of the family members was actually small, they showed that Yarkovsky drift itself accounted for most of the family's extension in semimajor axis. Assisted by the YORP effect, which over a YORP-cycle timescale tilts obliquities toward extreme values, the Yarkovsky effect (dominated by its diurnal component) is maximized, and pushes small family members toward the extreme values in a_p. If properly modeled, this method allows us to approximately constrain the interval of time needed since the family-forming event to reach the observed extension (Fig. 7). Several applications of this method can be found in *Vokrouhlický et al.* (2006a,b,c), *Bottke et al.* (2007), *Carruba* (2009), or *Carruba and Morbidelli* (2011). Recently *Bottke et al.* (2015) noticed that the classical setting of this method does not permit a satisfactory solution for the low-albedo, inner-belt Eulalia family. Their proposed modification requires an extended time spent by small asteroids in the extreme obliquity state, which in turn requires a simultaneous slowdown in the evolution of their rotation rates by the YORP effect. In fact, this may be readily obtained by postulating that the YORP strength changes on a timescale shorter than the YORP cycle, an assumption that may follow from the extreme sensitivity of the YORP effect to asteroid shape [the self-limitation effect discussed in section 2.1; see also *Cotto-Figueroa et al.* (2015)]. It is not clear, however, why this phenomenon should manifest itself primarily in this particular family, or whether it generally concerns all families ~1 b.y. old.

The model of Vokrouhlický et al. inherently contains a prediction that the small members in the "eared" families have preferred obliquity values (such that prograde-rotating objects occupy regions in the family with largest a values, and vice versa). Interestingly, recent works of *Hanuš et al.* (2013b) and *Kryszczyńska* (2013) confirm this trend in the cases of several families, and more detailed studies are underway.

A peculiar situation arises for families embedded in the first-order mean-motion resonances with Jupiter. In these cases, the resonant lock prohibits large changes in the

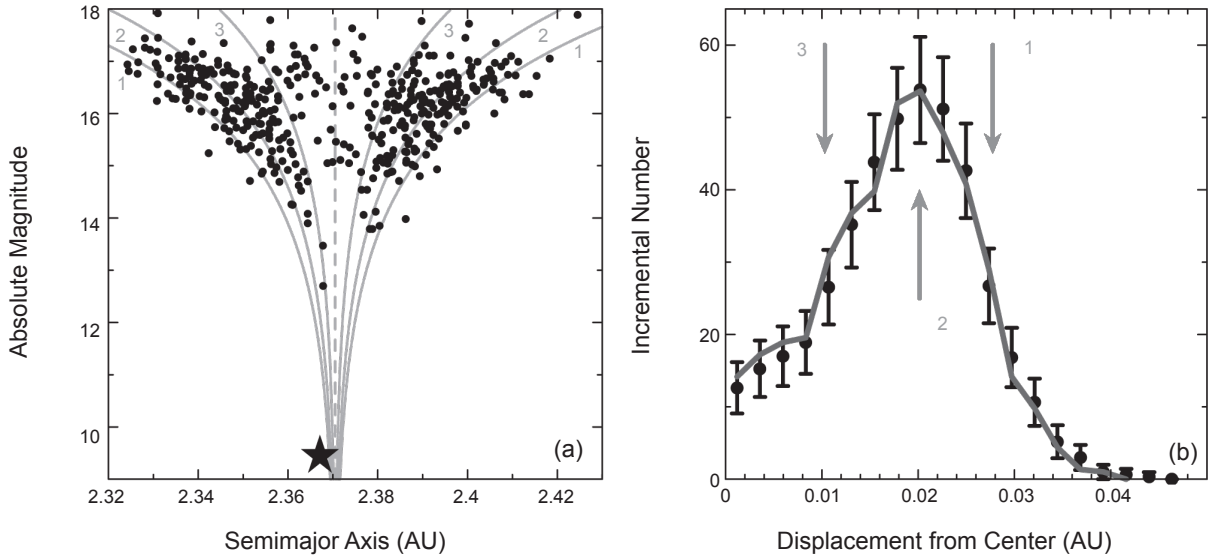

Fig. 7. (a) The Erigone family members projected on the plane of the proper semimajor axis a_P and the absolute magnitude H; 432 numbered family members, including (163) Erigone (star), are shown as black symbols. The gray lines show 0.2 H = log(|a_P–a_0|/C), with a_0 = 2.3705 AU and three different values of the C parameter labeled 1, 2, and 3. **(b)** Fixing the H level (16 mag in our case) results in a one-to-one link between the C value and a displacement from the center a_0, shown here at the abscissa. The symbols represent the Erigone family using a statistical distribution in the C-bins (assuming a symmetry C → –C in this case); uncertainty is simply $\sqrt{N}$, where N is the number of asteroids in the bin. A numerical model (dark gray line) seeks to match the distribution by adjusting several free parameters such as the family age and initial dispersal of fragments from the largest fragment. The gray arrows point to the corresponding C = const. lines on **(a)**. Adapted from *Vokrouhlický et al.* (2006a), with the family update as of April 2014.

semimajor axis, but the Yarkovsky effect manifests itself by a secular increase or decrease of the eccentricity. Modeling of this evolution allowed *Brož and Vokrouhlický* (2008) and *Brož et al.* (2011) to estimate the age of the Schubart and Hilda families located in the 3:2 mean-motion resonance with Jupiter.

5. APPLICATIONS OF THE YORP AND BINARY YORP EFFECTS

5.1. Distribution of Rotation Rate and Obliquity for Small Asteroids

As explained in section 2.1, a secular change in rotation rate and obliquity are the two main dynamical implications of the YORP effect. Therefore, it is has been natural to seek traits of these trends among the populations of small asteroids. Luckily, the amount of data and their quality have significantly increased over the last decade and allowed such analyses.

5.1.1. Rotation-rate distribution. The distribution of rotation frequencies of large asteroids in the main belt matches a Maxwellian function quite well with a mean rotation period of ~8–12 h, depending on the size of the bin used. However, data for asteroids smaller than ~20 km show significant deviations from this law, with many asteroids either having very slow or very fast rotation rates. Note that similar data are also available for NEAs, but the main-belt sample is more suitable because its interpretation is not complicated by possible effects of planetary close approaches. After eliminating known or suspected binary systems, solitary kilometer-sized asteroids in the main asteroid belt were shown to have a roughly uniform distribution of rotation frequencies (*Pravec et al.,* 2008) (Fig. 8). The only statistically significant deviation was an excess of slow rotators (periods less than a day or so). Note that the sample described by *Pravec et al.* (2008) is superior to other existing datasets so far in elimination of all possible survey biases [which may prevent recognition of slow rotators (P. Pravec, personal communication)].

These results are well explained with a simple model of a relaxed YORP evolution. In this view asteroid spin rates are driven by the YORP effect toward extreme (large or small) values on a characteristic (YORP) timescale dependent on the size. Asteroids evolving toward a state of rapid rotation shed mass and thus put a brake on their rotation rate, while those who slow their rotation too much enter into a tumbling phase. They may later emerge from this state naturally, with a new spin vector, or may gain rotation angular momentum by subcatastrophic impacts. After a few cycles the spin rates settle to an approximately uniform distribution and the memory of its initial value is erased. In fact, the observations similar to those shown in Fig. 8 may help to quantitatively calibrate the processes that allow bodies to reemerge from the slow-rotating state.

Statler et al. (2013) presented a first attempt to obtain unbiased rotation properties of very small NEAs. They found

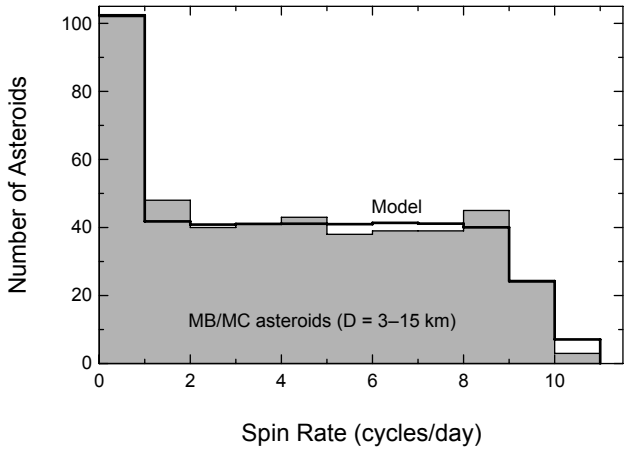

Fig. 8. Spin rate distribution of 462 small main-belt and Mars-crossing asteroids (sizes in the 3–15-km range, with a median value of 6.5 km). The distribution is flat with only two features: (1) an excess of slow rotators with periods longer than 1 d (the first bin), and (2) a linear decrease on the 8–10 cycles d^{-1} interval. The latter is simply due to rotational fission limit dependence on the actual shape of the body, while the former holds information how the spin reemerges from the slow-rotation limit. Results from a simple model of a YORP-relaxed population of objects is shown in black (model). Adapted from *Pravec et al.* (2008), with an update from P. Pravec as of April 2014.

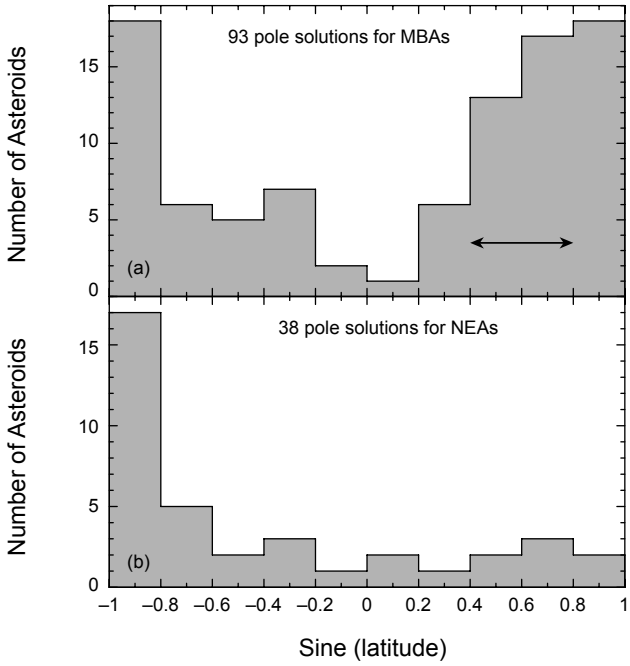

Fig. 9. (a) Distribution of ecliptic pole latitude for 93 small main-belt asteroids (MBAs; sizes less than 30 km). The arrow indicates the zone of prograde-rotating objects potentially affected by the spin-orbit resonances (e.g., *Vokrouhlický et al.,* 2006d). This effect is nonexistent for retrograde-rotating objects and the poles are let to drift closer to the extreme value. **(b)** Distribution of ecliptic pole latitude for 38 near-Earth asteroids (NEAs). This is dominated by retrograde-rotating objects (≃73% cases), because this sense of rotation offers a better chance to migrate to the planet-crossing space. In both cases, the tendency to extreme latitude values is due to the YORP effect. MBA data adapted from *Hanuš et al.* (2013a), NEA data from the Asteroid Lightcurve Database (LCDB) compilation as of February 2014.

an anomalously large fraction of very fast rotating bodies in the <60-m group, which may witness a preferential ability of YORP to accelerate the rotation rate of small asteroids. A larger sample, less vulnerable to potential errors and biases, will be needed to verify this potentially important result.

5.1.2. Obliquity distribution. Similarly, the distribution of pole orientation of large asteroids in the main belt is roughly isotropic, with only a moderate excess of prograde rotating bodies. On the other hand, rotation poles of small asteroids (sizes ≤30 km) are strongly concentrated toward ecliptic south and north poles (*Hanuš et al.,* 2013a) (Fig. 9). Note that this trend is better exhibited in the retrograde-rotating group (obliquities >90°), because the prograde-rotating asteroids are perturbed by secular spin-orbit resonances (e.g., *Vokrouhlický et al.,* 2006d). As a result, there is more mixing among the obliquities <90°, which causes their flatter distribution in Fig. 9. Overall, this result can again be matched with the above-mentioned simple model of YORP evolution, because YORP torques drive obliquity toward its extreme values (e.g., *Čapek and Vokrouhlický,* 2004).

The pole distribution of NEAs, in spite of a still limited sample, indicates a strong preference of directions near the south ecliptic pole (*La Spina et al.,* 2004) (Fig. 9). The ratio between the number of retrograde- vs. prograde-rotating bodies is nearly 3:1. This is in a very good agreement with prediction from a model, where most NEAs are delivered from the main belt via principal resonant routes, secular ν_6 resonance, and 3:1 mean-motion resonance with Jupiter (*Bottke et al.,* 2002b), resupplied by the Yarkovsky effect (*Morbidelli and Vokrouhlický,* 2003). This is because while the 3:1 resonance may be reached from heliocentric orbits with both larger and smaller value of the semimajor axis, asteroids can enter the ν_6 resonance only by decreasing their semimajor axis. Taking into account the proportion by which these resonances contribute to the NEA population (*Bottke et al.,* 2002b), one obtains the observed 3:1 ratio between spin retrograde vs. prograde rotators. This obviously assumes that the rotation pole directions do not become significantly modified after the asteroids enter the planet-crossing zone.

Another interesting piece of information comes from a study of orbital pole distribution of small binary systems in the main belt. *Pravec et al.* (2012) show that poles of these systems are non-isotropic with strong concentration toward the ecliptic poles, thus mimicking the spin distribution of solitary asteroids in the same class. This picture is consistent with a model in which these small binaries are formed by fission of the parent body, whose rotation has been brought to the rotational limit by the YORP effect.

5.2. Asteroids with Rotation Axes Caught in Spin-Orbit Resonances

In an attempt to generalize Cassini's second and third laws, Giuseppe Colombo developed a mathematical model in the 1960s that describes the evolution of a body's spin axis rotating about a principal axis of its inertia tensor (*Colombo,* 1966). Colombo included two fundamental elements in his approach: (1) gravitational torques due to a massive center (e.g., the Sun), and (2) regular precession of the orbital plane of the body by exterior perturbers (e.g., planets). Because approach (1) produces a regular precession of the spin axis, a secular spin-orbit resonance (with a stable fixed point called Cassini state 2) may occur between its frequency and the frequency by which the orbital plane precesses in the inertial space. Such a resonance may occur only for a certain range of obliquity and rotation period values, and thus there is only a small probability that the spin state of any given asteroid is located in the Cassini state 2 associated with one of the frequencies by which its orbital plane precesses in space.

With this as background, the discovery of five prograde-rotating Koronis member asteroids with similar spin vectors (i.e., spin axes nearly parallel in inertial space and similar rotation periods) was a surprise. Additionally, the sample of retrograde-rotating asteroids in the same observation campaign showed obliquities anomalously large (≥154°) and either short or long rotation periods (*Slivan,* 2002; *Slivan et al.,* 2009). This puzzling situation, however, was solved with a model where the gravitational spin dynamics were complemented with the long-term effects of YORP torques (*Vokrouhlický et al.,* 2003). The YORP effect was shown to bring, on a ~2–3-G.y. timescale, prograde states close to Cassini state 2 associated with the prominent s_6 frequency in the orbital precession, thus providing a natural explanation for the alignment in inertial space. Note that while the capture is fundamentally unstable, the evolution becomes slowed down near the observed obliquities where the YORP effect changes rotation period only slowly (section 2.1). No resonant trapping zone exists for retrograde-rotating bodies, whose evolution is thus simpler and, driven solely by the YORP effect, evolve toward extreme values in both their obliquities and rotation periods.

The possibility exists for asteroid spin states to be trapped in similar spin-orbit resonant states, dubbed "Slivan states," for bodies residing on low-inclination orbits, especially in the central and outer parts of the main asteroid belt. Recently reported Slivan states in the inner part of the belt, namely in the Flora region (*Kryszczyńska,* 2013), are questionable because of their instability. Yet model refinement would be clearly needed if more bodies are observed near these states in the Flora region (*Vraštil and Vokrouhlický,* 2015).

5.3. Formation and Long-Term Evolution of Binary Systems

The BYORP effect is predicted to play a fundamental role in the evolution of asteroid binaries. As noted earlier, it has been hypothesized that nearly all observed small, rubble-pile binary asteroid systems lie in an equilibrium state where BYORP and tidal torques are balanced.

The BYORP effect plays many other roles in controlling the evolution of a binary asteroid. *Jacobson and Scheeres* (2011a) studied the evolution of asteroid systems arising from the rotational fission of a primary body (due to YORP torques). While the initial creation of a stable binary system is a complex process (see the chapter by Walsh and Jacobson in this volume), once a stable binary forms with at least one of the bodies being synchronous, the BYORP effect can take control of its subsequent evolution. There are several different pathways, which we briefly review here.

First, if the ratio between the secondary and primary is greater than ~0.2, the system is expected to eventually settle into a double-synchronous binary asteroid such as (69230) Hermes. In this configuration both of the synchronous bodies can contribute to the BYORP effect, either working together to contract or expand the system, or working against each other. In none of these cases is it expected that the system will settle into a stable equilibrium, as migration would only stop if the two BYORP effects counteract each other exactly. Similarly, there are no significant tidal dissipation effects once a system is doubly synchronous, and thus the case of contraction will lead directly to collapse (e.g., *Taylor and Margot,* 2014). The expansion phase of a doubly synchronous binary asteroid has not been investigated in detail as of yet in terms of physical evolution. However, as the system becomes larger, it should be more susceptible to other exogenous perturbations (e.g., *Fang and Margot,* 2012).

For stable binaries that have a mass ratio <0.2 between the secondary and primary, the evolutionary path is seen to be quite different (see also the chapter by Walsh and Jacobson in this volume). If a stable binary is formed, it is generally a singly synchronous system with the secondary in a synchronous state and the primary rotating faster than the spin rate. If the secondary's BYORP coefficient is negative and the system contracts, then it should migrate into a BYORP-tide equilibrium. Once in this state it may persist for long periods of time, as the system has been hardened against exogenous perturbations due to its more compact state (e.g., *Fang and Margot,* 2012). A noticeable outcome is that the primary body should lose spin rate, due to the tidal transfer of torque. However, the primary may still be subject to the YORP effect and thus may not exhibit a clear slowing of its spin rate.

If the secondary's BYORP coefficient is positive, the system expands, with tides now working in the same direction. In this case there is also an interesting interplay between the libration of the secondary about its synchronous state and tidal dissipation that acts to damp out such librations. In the expansive case without librational damping, the amplitude of libration is expected to increase as the orbit increases, due to an adiabatic integral involving the libration state (e.g., *Jacobson et al.,* 2014). How these two effects combine can control when the secondary can lose synchronous lock, causing the BYORP effect to shut down. The model and

simulations developed in *Jacobson et al.* (2014) indicate that synchronicity is lost at a far enough distance so that further tidal evolution of the system does not occur, and the system can be described as a wide-asynchronous binary. This paper makes favorable comparisons between predictions of the theory and such observed binary systems. An alternate, earlier theory was proposed by *Ćuk and Nesvorný* (2010) in which the expanding system can become trapped in a resonance with the eccentricity of the orbit growing secularly. They hypothesized that such a system would then lose synchronicity, but subsequently relax back into synchronous rotation several times until the system enters a contractive phase. The very different predictions from these models indicate that the full interaction of such expanding binary systems is not yet fully understood.

In addition to expansion and contraction effects, there may also be out-of-plane BYORP effects that cause migration of the binary system's orbit pole, similar to the YORP effect (see *Ćuk and Burns,* 2005). *Steinberg and Sari* (2011) further studied these situations and proposed that, similar to YORP, the obliquity states should preferentially migrate toward some asymptotic values (either 0°, 90°, or 180° in their model). *Ćuk* (2007) noted that this effect, when combined with the characteristic zero-crossing of the BYORP coefficient as a function of obliquity, could create an accumulation of binaries at obliquities between these limits. It should also be mentioned that *McMahon and Scheeres* (2010b) did not predict an inclination evolution due to the BYORP effect, owing to the effects of the primary oblateness. Thus, it is apparent that the obliquity migration of a binary orbit due to BYORP is not fully understood or settled, and remains a ripe topic for further investigation.

6. CONCLUSION AND FUTURE WORK

As with many mature disciplines in science, studies of the Yarkovsky and YORP effects have their own agenda of development in the future years. What makes them even more appealing is that some of these future results have interesting implications for other domains in planetary astronomy. Here we try to summarize at least a few examples.

While it seems nearly certain that numerous detections of the Yarkovsky effect will emerge from current and upcoming astrometric surveys in the next decade (e.g., *Delbò et al.,* 2008; *Mouret and Mignard,* 2011; *Nugent et al.,* 2012b; *Desmars,* 2015), more work is needed to secure YORP detections, especially across the whole range of possible rotation periods. This should help us understand in what proportion the YORP effect results in acceleration or deceleration of the rotation rate.

The binary YORP detections are in their infancy but will become an important topic of future research. This is because the BYORP effect is an essential element, as far as we understand it today, in orbital evolution of binary asteroids. Detections, or continuing nondetections, of the expected BYORP signal will have implications not only for the orbital evolution pathways of binaries and their physical parameters, but also for estimates of their lifetime and formation rate.

As the rotations of asteroids become slower by the YORP effect, they naturally enter the tumbling state. The available models so far, whether analytical or numerical in nature (*Vokrouhlický et al.,* 2007; *Cicalò and Scheeres,* 2010; *Breiter et al.,* 2011), indicate that the YORP effect keeps navigating the rotation through the tumbling phase space without an easy return to the rotation about the shortest axis of the inertia tensor. Yet, more than 90% of asteroids do rotate in the shortest-axis mode. A solution for this conundrum is not yet clear and warrants further work. The above-mentioned models of the YORP effect in the tumbling regime neglect thermal inertia, which may be an important factor. Additionally, no detailed model combining the YORP effect and the effects of inelastic energy dissipation inside the body has been presented [although the initial work does not seem to remedy the problem (*Breiter and Murawiecka,* 2015)].

While it is generally accepted that the YORP effect is the driving dynamical process that brings small asteroids to their fission, more work is needed to understand how the fission mechanics really work. Along the path to the fission limit, the body may undergo structural and shape changes that could either help the fission process, or potentially invert the YORP acceleration to effectively prevent fission. It is not known which of these alternatives typically dominates and in what proportion. This, again, could have important implications for the formation rate of both small binaries and asteroid pairs. Additionally, this would help us to better understand the YORP self-limitation processes and the way in which they potentially modify classical YORP results.

Acknowledgments. The authors are grateful to D. Farnocchia for assistance in the compilation of Table 1 and P. Pravec for providing data shown in Fig. 8. We also thank reviewers D. P. Rubincam and B. Rozitis for their suggestions, which helped to improve the original form of the chapter. The work of D.V. was partially supported by the Czech Grant Agency (grant P209-13-01308S). The participation of W.F.B. was supported by NASA's Solar System Evolution Research Virtual Institute (SSERVI) program through a grant to the Institute for the Science of Exploration Targets at the Southwest Research Institute in Boulder, Colorado. The work of S.R.C. was conducted at the Jet Propulsion Laboratory, California Institute of Technology, under a contract with NASA. T.S.S. acknowledges support from NASA Planetary Geology and Geophysics grant NNX11AP15G.

REFERENCES

Afonso G. B., Gomes R. S., and Florczak M. A. (1995) Asteroid fragments in Earth-crossing orbits. *Planet. Space Sci., 43,* 787–795.

Beekman G. (2006) I. O. Yarkovsky and the discovery of 'his' effect. *J. Hist. Astron., 37,* 71–86.

Bottke W. F., Vokrouhlický D., Brož M., Nesvorný D., and Morbidelli A. (2001) Dynamical spreading of asteroid families via the Yarkovsky effect: The Koronis family and beyond. *Science, 294,* 1693–1696.

Bottke W. F., Vokrouhlický D., Rubincam D. P., and Brož M. (2002a) Dynamical evolution of asteroids and meteoroids using the Yarkovsky effect. In *Asteroids III* (W. F. Bottke Jr. et al., eds.), pp. 395–408. Univ. of Arizona, Tucson.

Bottke W. F., Morbidelli A., Jedicke R., et al. (2002b) Debiased orbital and absolute magnitude distribution of the near-Earth objects. *Icarus, 156,* 399–433.

Bottke W. F., Vokrouhlický D., Rubincam D. P., and Nesvorný D. (2006) The Yarkovsky and YORP effects: Implications for asteroid dynamics. *Annu. Rev. Earth Planet. Sci., 34,* 157– 191.

Bottke W. F., Vokrouhlický D., and Nesvorný D. (2007) An asteroid breakup 160 My ago as a probable source of the K-T impactor. *Nature, 449,* 48–53.

Bottke W. F. Vokrouhlický D., Walsh K., et al. (2015) In search of the source of asteroid (101955) Bennu: Application of the stochastic YORP model. *Icarus, 247,* 191–217.

Breiter S. and Michałska H. (2008) YORP torque as the function of shape harmonics. *Mon. Not. R. Astron. Soc., 388,* 927–944.

Breiter S. and Murawiecka M. (2015) Tumbling asteroid rotation with the YORP torque and inelastic energy dissipation. *Mon. Not. R. Astron. Soc., 449,* 2489–2497.

Breiter S. and Vokrouhlický D. (2011) YORP effect with anisotropic radiation. *Mon. Not. R. Astron. Soc., 410,* 2807–2816.

Breiter S., Michałska H., Vokrouhlický D., and Borczyk W. (2007) Radiation induced torques on spheroids. *Astron. Astrophys., 471,* 345–353.

Breiter S., Bartczak P., Czekaj M., Oczujda B., and Vokrouhlický D. (2009) The YORP effect on 25143 Itokawa. *Astron. Astrophys., 507,* 1073–1081.

Breiter S., Vokrouhlický D., and Nesvorný D. (2010a) Analytical YORP torques model with an improved temperature distribution function. *Mon. Not. R. Astron. Soc., 401,* 1933–1949.

Breiter S., Bartczak P., and Czekaj M. (2010b) YORP torques with 1D thermal model. *Mon. Not. R. Astron. Soc., 408,* 1576–1589.

Breiter S., Rożek A., and Vokrouhlický D. (2011) YORP effect on tumbling objects. *Mon. Not. R. Astron. Soc., 417,* 2478–2499.

Brož M. and Vokrouhlický D. (2008) Asteroids in the first order resonances with Jupiter. *Mon. Not. R. Astron. Soc., 390,* 715–732.

Brož M., Vokrouhlický D., Morbidelli A., Nesvorný D., and Bottke W. F. (2011) Did the Hilda collisional family form during the late heavy bombardment? *Mon. Not. R. Astron. Soc., 414,* 2716–2727.

Čapek D. and Vokrouhlický D. (2004) The YORP effect with finite thermal conductivity. *Icarus, 172,* 526–536.

Carruba V. (2009) The (not so) peculiar case of the Padua family. *Mon. Not. R. Astron. Soc., 395,* 358–377.

Carruba V. and Morbidelli A. (2011) On the first ν_6 anti-aligned librating asteroid family of Tina. *Mon. Not. R. Astron. Soc., 412,* 2040–2051.

Chesley S. R., Ostro S. J., Vokrouhlický D., et al. (2003) Direct detection of the Yarkovsky effect via radar ranging to the near-Earth asteroid 6489 Golevka. *Science, 302,* 1739–1742.

Chesley S. R., Vokrouhlický D., Ostro S. J., et al. (2008) Direct estimation of Yarkovsky accelerations on near-Earth asteroids. In *Asteroids, Comets, Meteors,* Abstract #8330. Lunar and Planetary Institute, Houston.

Chesley S. R., Farnocchia D., Nolan M. C., et al. (2014) Orbit and bulk density of the OSIRIS-REx target asteroid (101955) Bennu. *Icarus, 235,* 5–22.

Cicalò S. and Scheeres D. J. (2010) Averaged rotational dynamics of an asteroid in tumbling rotation under the YORP torque. *Cel. Mech. Dyn. Astron., 106,* 301–337.

Colombo G. (1966) Cassini's second and third laws. *Astron. J., 71,* 891–896.

Cotto-Figueroa D., Statler T. S., Richardson D. C., and Tanga P. (2015) Coupled spin and shape evolution of small rubble-pile asteroids: Self-limitation of the YORP effect. *Astrophys. J., 803,* 25.

Ćuk M. (2007) Formation and destruction of small binary asteroids. *Astrophys. J. Lett., 659,* L57–L60.

Ćuk M. and Burns J. A. (2005) Effects of thermal radiation on the dynamics of binary NEAs. *Icarus, 176,* 418–431.

Ćuk M. and Nesvorný D. (2010) Orbital evolution of small binary asteroids. *Icarus, 207,* 732–743.

Delbò M., Tanga P., and Mignard F. (2008) On the detection of the Yarkovsky effect on near-Earth asteroids by means of Gaia. *Planet. Space Sci., 56,* 1823–1827.

Desmars J. (2015) Detection of Yarkovsky acceleration in the context of precovery observations and the future Gaia catalogue. *Astron. Astrophys*., *575,* A53.

Ďurech J. (2005) 433 Eros — comparison of lightcurve extrema from 1901–1931 with the present rotation state. *Astron. Astrophys., 431,* 381–383.

Ďurech J., Vokrouhlický D., Kaasalainen M., et al. (2008a) Detection of the YORP effect for asteroid (1620) Geographos. *Astron. Astrophys., 489,* L25–L28.

Ďurech J., Vokrouhlický D., Kaasalainen M., et al. (2008b) New photometric observations of asteroids (1862) Apollo and (25143) Itokawa — analysis of YORP effect. *Astron. Astrophys., 488,* 345–350.

Ďurech J., Vokrouhlický D., Baransky A. R., et al. (2012) Analysis of the rotation period of asteroids (1865) Cerberus, (2100) Ra-Shalom and (3103) Eger — search for the YORP effect. *Astron. Astrophys., 547,* A10.

Fang J. and Margot J.-L. (2012) Near-Earth binaries and triples: Origin and evolution of spin-orbital properties. *Astron. J., 143,* 24.

Farinella P., Vokrouhlický D., and HartmannW. K. (1998) Meteorite delivery via Yarkovsky orbital drift. *Icarus, 132,* 378–387.

Farnocchia D., and Chesley S. R. (2014) Assessment of the 2880 impact threat from asteroid (29075) 1950 DA. *Icarus, 229,* 321–327.

Farnocchia D., Chesley S. R., Chodas P. W., Micheli M., Tholen D. J., Milani A., Elliott G. T., and Bernardi F. (2013a) Yarkovsky-driven impact risk analysis for asteroid (99942) Apophis. *Icarus, 224,* 192–200.

Farnocchia D., Chesley S. R., Vokrouhlický D., Milani A., Spoto F., and Bottke W. F. (2013b) Near Earth asteroids with measurable Yarkovsky effect. *Icarus, 224,* 1–13.

Goldreich P. and Sari R. (2009) Tidal evolution of rubble piles. *Astrophys. J., 691,* 54–60.

Golubov O. and Krugly Y. N. (2012) Tangential component of the YORP effect. *Astrophys. J. Lett., 752,* L11.

Golubov O., Scheeres D. J., and Krugly Y. N. (2014) A three-dimensional model of tangential YORP. *Astrophys. J., 794,* 22.

Hanuš J., Ďurech J., Brož M., et al. (2013a) Asteroids' physical models from combined dense and sparse photometry and scaling of the YORP effect by the observed obliquity distribution. *Astron. Astrophys., 551,* A67.

Hanuš J., Brož M., Ďurech J., et al. (2013b) An anisotropic distribution of spin vectors in asteroid families. *Astron. Astrophys., 559,* A134.

Hapke B. (1993) *Theory of Reflectance and Emittance Spectroscopy.* Cambridge Univ., Cambridge.

Hudson R. S., and Ostro S. J. (1995) Shape and non-principal axis spin state of asteroid 4179 Toutatis. *Science, 270,* 84–86.

Jacobson S. A. and Scheeres D. J. (2011a) Dynamics of rotationally fissioned asteroids: Source of observed small asteroid systems. *Icarus, 214,* 161–178.

Jacobson S. A. and Scheeres D. J. (2011b) Long-term stable equilibria for synchronous binary asteroids. *Astrophys. J. Lett., 736,* L19.

Jacobson S. A., Scheeres D. J., and McMahon J. (2014) Formation of the wide asynchronous binary asteroid population. *Astrophys. J., 780,* 60.

Kaasalainen M. and Nortunen H. (2013) Compact YORP formulation and stability analysis. *Astron. Astrophys., 558,* A104.

Kaasalainen M., Ďurech J., Warner B. D., Krugly Y. N., and Gaftonyuk N. M. (2007) Acceleration of the rotation of asteroid 1862 Apollo by radiation torques. *Nature, 446,* 420–422.

Kryszczyńska A. (2013) Do Slivan states exist in the Flora family? II. Fingerprints of the Yarkovsky and YORP effects. *Astron. Astrophys., 551,* A102.

La Spina A., Paolicchi P., Kryszczyńska A., and Pravec P. (2004) Retrograde spins of near-Earth asteroids from the Yarkovsky effect. *Nature, 428,* 400–401.

Lauretta D. S., Barucci M. A., Binzel R. P., et al. (2015) The OSIRIS-REx target asteroid (101955) Bennu: Constraints on its physical, chemical, and dynamical nature from astronomical observations. *Meteoritics & Planet. Sci., 50,* 834–849.

Lowry S. C., Fitzsimmons A., Pravec P., et al. (2007) Direct detection of the asteroidal YORP effect. *Science, 316,* 272–274.

Lowry S. C., Weissman P. R., Duddy S. R., et al. (2014) The internal structure of asteroid (25143) Itokawa as revealed by detection of YORP spin-up. *Astron. Astrophys., 562,* A48.

McMahon J. and Scheeres D. J. (2010a) Secular orbit variation due to solar radiation effects: A detailed model for BYORP. *Cel. Mech. Dyn. Astron., 106,* 261–300.

McMahon J. and Scheeres D. J. (2010b) Detailed prediction for the BYORP effect on binary near-Earth asteroid (66391) 1999 KW_4 and implications for the binary population. *Icarus, 209,* 494–509.
Milani A., Chesley S. R., Sansaturio M. E., Bernardi F., Valsecchi G. B., and Arratia O. (2009) Long term impact risk for (101955) 1999 RQ_{36}. *Icarus, 203,* 460–471.
Mommert M., Hora J. L., Farnocchia D., et al. (2014) Constraining the physical properties of near-Earth object 2009 BD. *Astrophys. J., 786,* 148.
Morbidelli A. and Vokrouhlický D. (2003) The Yarkovsky driven origin of near-Earth asteroids. *Icarus, 163,* 120–134.
Mouret S. and Mignard F. (2011) Detecting the Yarkovsky effect with the Gaia mission: List of the most promising candidates. *Mon. Not. R. Astron. Soc., 413,* 741–748.
Nesvorný D. and Bottke W. F. (2004) Detection of the Yarkovsky effect for main-belt asteroids. *Icarus, 170,* 324–342.
Nesvorný D. and Vokrouhlický D. (2006) New candidates for recent asteroid breakups. *Astron. J., 132,* 1950–1958.
Nesvorný D. and Vokrouhlický D. (2007) Analytic theory of the YORP effect for near-spherical objects. *Astron. J., 134,* 1750–1768.
Nesvorný D. and Vokrouhlický D. (2008a) Analytic theory for the YORP effect on obliquity. *Astron. J., 136,* 291–299.
Nesvorný D. and Vokrouhlický D. (2008b) Vanishing torque from radiation pressure. *Astron. Astrophys., 480,* 1–3.
Nesvorný D., Bottke W. F., Dones L., and Levison H. F. (2002) The recent breakup of an asteroid in the main-belt region. *Nature, 417,* 720–722.
Nesvorný D., Bottke W. F., Levison H. F., and Dones L. (2003) Recent origin of the zodiacal dust bands. *Astrophys. J., 591,* 486–497.
Nesvorný D., Vokrouhlický D., and Bottke W. F. (2006) A main belt asteroid break-up 450 ky ago. *Science, 312,* 1490.
Nesvorný D., Bottke W. F., Vokrouhlický D., Sykes M., Lien D. J., and Stansberry J. (2008) Origin of the near-ecliptic zodiacal dust band. *Astrophys. J. Lett., 679,* L143–L146.
Nesvorný D., Vokrouhlický D., Morbidelli A., and Bottke W. F. (2009) Asteroidal source of L chondrite meteorites. *Icarus, 200,* 698–701.
Novaković B. (2010) Portrait of Theobalda as a young asteroid family. *Mon. Not. R. Astron. Soc., 407,* 1477–1486.
Novaković B., Dell'Oro A., Cellino A., and Knežević Z. (2012) Recent collisional jet from a primitive asteroid. *Mon. Not. R. Astron. Soc., 425,* 338–346.
Novaković B., Hsieh H. H., Cellino A., Micheli M., and Pedani M. (2014) Discovery of a young asteroid cluster associated with P/2012 F5 (Gibbs). *Icarus, 231,* 300–309.
Nugent C. R., Margot J. L., Chesley S. R., and Vokrouhlický D. (2012a) Detection of semi-major axis drifts in 54 near-Earth asteroids. *Astron. J., 144,* 60.
Nugent C. R., Mainzer A., Masiero J., Grav T., and Bauer J. (2012b) The Yarkovsky drift's influence on NEAs: Trends and predictions with NEOWISE measurements. *Astron. J., 144,* 75.
Öpik E. J. (1951) Collision probabilities with the planets and the distribution of interplanetary matter. *Proc. R. Irish Acad., A54,* 165–199.
Ostro S. J., Margot J.-L., Benner L. A. M., et al. (2006) Radar imaging of binary near-Earth asteroid (66391) 1999 KW_4. *Science, 314,* 1276–1280.
Paddack S. J. (1969) Rotational bursting of small celestial bodies: Effects of radiation pressure. *J. Geophys. Res., 74,* 4379–4381.
Paddack S. J. and Rhee J. W. (1975) Rotational bursting of interplanetary dust particles. *Geophys. Res. Lett., 2,* 365–367.
Peterson C. (1976) A source mechanism for meteorites controlled by the Yarkovsky effect. *Icarus, 29,* 91–111.
Pravec P., Harris A. W., Vokrouhlický D., et al. (2008) Spin rate distribution of small asteroids. *Icarus, 197,* 497–504.
Pravec P., Vokrouhlický D., Polishook D., et al. (2010) Asteroid pairs formed by rotational fission. *Nature, 466,* 1085–1088.
Pravec P., Scheirich P., Vokrouhlický D., et al. (2012) Binary asteroid population. II. Anisotropic distribution of orbit poles. *Icarus, 218,* 125–143.
Pravec P., Scheirich P., Ďurech J., et al. (2014) The tumbling spin state of (99942) Apophis. *Icarus, 233,* 48–60.
Radzievskii V. V. (1952) The influence of anisotropy of reemitted sunlight on the orbital motion of asteroids and meteoroids. *Astron. Zh., 29,* 162–170.
Radzievskii V. V. (1954) A mechanism for the disintegration of asteroids and meteorites. *Dokl. Akad. Nauk SSSR, 97,* 49–52.
Richardson D. C., Elankumaran P., and Sanderson R. E. (2005) Numerical experiments with rubble piles: Equilibrium shapes and spins. *Icarus, 173,* 349–361.
Rozitis B. and Green S. F. (2012) The influence of rough surface thermal-infrared beaming on the Yarkovsky and YORP effects. *Mon. Not. R. Astron. Soc., 423,* 367–388.
Rozitis B. and Green S. F. (2013) The influence of global self-heating on the Yarkovsky and YORP effects. *Mon. Not. R. Astron. Soc., 433,* 603–621.
Rozitis B. and Green S. F. (2014) Physical characterization of near-Earth asteroid (1620) Geographos. Reconciling radar and thermal-infrared observations. *Astron. Astrophys., 568,* A43.
Rozitis B., Duddy S. R., Green S. F., and Lowry S. C. (2013) A thermophysical analysis of the (1862) Apollo Yarkovsky and YORP effects. *Astron. Astrophys., 555,* A20.
Rozitis B., MacLennan E., and Emery J. P. (2014) Cohesive forces prevent the rotational breakup of rubble-pile asteroid (29075) 1950 DA. *Nature, 512,* 174–176.
Rubincam D. P. (1982) On the secular decrease in the semimajor axis of LAGEOS's orbit. *Cel. Mech., 26,* 361–382.
Rubincam D. P. (1995) Asteroid orbit evolution due to thermal drag. *J. Geophys. Res., 100,* 1585–1594.
Rubincam D. P. (1998) Yarkovsky thermal drag on small asteroids and Mars-Earth delivery. *J. Geophys. Res., 103,* 1725–1732.
Rubincam D. P. (2000) Radiative spin-up and spin-down of small asteroids. *Icarus, 148,* 2–11.
Rubincam D. P. and Paddack S. J. (2010) Zero secular torque on asteroids from impinging solar photons in the YORP effect: A simple proof. *Icarus, 209,* 863–865.
Scheeres D. J. (2007) The dynamical evolution of uniformly rotating asteroids subject to YORP. *Icarus, 188,* 430–450.
Scheeres D. J. (2015) Landslides and mass shedding on spinning spheroidal asteroids. *Icarus, 247,* 1–17.
Scheeres D. J. and Gaskell R. W. (2008) Effect of density inhomogeneity on YORP: The case of Itokawa. *Icarus, 198,* 125–129.
Scheeres D. J. and Mirrahimi S. (2008) Rotational dynamics of a solar system body under solar radiation torques. *Cel. Mech. Dyn. Astron., 100,* 69–103.
Scheeres D. J., Abe M., Yoshikawa M., Nakamura R., Gaskell R. W., and Abell P. A. (2007) The effect of YORP on Itokawa. *Icarus, 188,* 425–429.
Scheeres D. J., Hartzell C. M., Sánchez P., and Swift M. (2010) Scaling forces to asteroid surfaces: The role of cohesion. *Icarus, 210,* 968–984.
Scheirich P., Pravec P., Jacobson S. A., et al. (2015) The binary near-Earth asteroid (175706) 1996 FG_3 — An observational constraint on its orbital stability. *Icarus, 245,* 56–63.
Schwartz S. R., Richardson D. C., and Michel P. (2012) An implementation of the soft-sphere discrete element method in a high-performance parallel gravity tree-code. *Granular Matter, 14,* 363–380.
Ševeček P., Brož M., Čapek D., and Ďurech J. (2015) The thermal emission from boulders on (25143) Itokawa and general implications for the YORP effect. *Mon. Not. R. Astron. Soc., 450,* 2104–2115.
Sekiya M. and Shimoda A. A. (2013) An iterative method for obtaining a nonlinear solution for the temperature distribution of a rotating spherical body revolving in a circular orbit around a star. *Planet. Space Sci., 84,* 112–121.
Sekiya M. and Shimoda A. A. (2014) An iterative method for obtaining a nonlinear solution for the temperature distribution of a rotating spherical body revolving in an eccentric orbit. *Planet. Space Sci., 97,* 23–33.
Slivan S. M. (2002) Spin vector alignment of Koronis family asteroids. *Nature, 419,* 49–51.
Slivan S. M., Binzel R. P., Kaasalainen M., et al. (2009) Spin vectors in the Koronis family. II. Additional clustered spins, and one stray. *Icarus, 200,* 514–530.
Spitale J. and Greenberg R. (2001) Numerical evaluation of the general Yarkovsky effect: Effects on semimajor axis. *Icarus, 149,* 222–234.
Spitale J. and Greenberg R. (2002) Numerical evaluation of the general Yarkovsky effect: Effects on eccentricity and longitude of periapse. *Icarus, 156,* 211–222.

Statler T. S. (2009) Extreme sensitivity of the YORP effect to small-scale topography. *Icarus, 202,* 502–513.

Statler T. S., Cotto-Figueroa D., Riethmiller D. A., and Sweeney K. M. (2013) Size matters: The rotation rates of small near-Earth asteroids. *Icarus, 225,* 141–155.

Steinberg E. and Sari R. (2011) Binary YORP effect and evolution of binary asteroids. *Astron. J., 141,* 55.

Taylor P. A. and Margot J. L. (2014) Tidal end states of binary asteroid systems with a nonspherical component. *Icarus, 229,* 418–422.

Taylor P. A., Margot J. L., Vokrouhlický D., et al. (2007) Spin rate of asteroid (54509) 2000 PH_5 increasing due to the YORP effect. *Science, 316,* 274–277.

Taylor P. A., Nolan M. C., Howell E. S., et al. (2012) 2004 FG_{11}. *Central Bureau Electronic Telegram (CBET), 3091, 1.*

Vinogradova V. P. and Radzievskii V. V. (1965) The acceleration of the martian satellites and the stabilization of orbits of artificial satellites. *Astron. Zh., 42,* 424–432.

Vokrouhlický D. (1998a) Diurnal Yarkovsky effect for metersized asteroidal fragments' mobility I. Linear theory. *Astron. Astrophys., 335,* 1093–1100.

Vokrouhlický D. (1998b) Diurnal Yarkovsky effect for metersized asteroidal fragments' mobility II. Non-sphericity effects. *Astron. Astrophys., 338,* 353–363.

Vokrouhlický D. (1999) A complete linear model for the Yarkovsky thermal force on spherical asteroid fragments. *Astron. Astrophys., 344,* 362–366.

Vokrouhlický D. and Bottke W. F. (2001) The Yarkovsky thermal force on small asteroids and their fragments: Choosing the right albedo. *Astron. Astrophys., 371,* 350–353.

Vokrouhlický D. and Brož M. (1999) An improved model of the seasonal Yarkovsky force for the regolith-covered asteroid fragments. *Astron. Astrophys., 350,* 1079–1084.

Vokrouhlický D. and Čapek D. (2002) YORP-induced long-term evolution of the spin state of small asteroids and meteoroids. I. Rubincam's approximation. *Icarus, 159,* 449–467.

Vokrouhlický D. and Farinella P. (2000) Efficient delivery of meteorites to the Earth from a wide range of asteroid parent bodies. *Nature, 407,* 606–608.

Vokrouhlický D. and Milani A. (2000) Direct solar radiation pressure on the orbits of small near-Earth asteroids: Observable effects? *Astron. Astrophys., 362,* 746–755.

Vokrouhlický D. and Nesvorný D. (2008) Pairs of asteroids probably of common origin. *Astron. J., 136,* 280–290.

Vokrouhlický D. and Nesvorný D. (2009) The common roots of asteroids (6070) Rheinland and (54827) 2001 NQ_8. *Astron. J., 137,* 111–117.

Vokrouhlický D., Milani A., and Chesley S. R. (2000) Yarkovsky effect on near-Earth asteroids: Mathematical formulation and examples. *Icarus, 148,* 118–138.

Vokrouhlický D., Nesvorný D., and BottkeW. F. (2003) The vector alignments of asteroid spins by thermal torques. *Nature, 425,* 147–151.

Vokrouhlický D., Čapek D., Kaasalainen M., and Ostro S. J. (2004) Detectability of YORP rotational slowing of asteroid 25143 Itokawa. *Astron. Astrophys., 414,* L21–L24.

Vokrouhlický D., Čapek D., Chesley S. R., and Ostro S. J. (2005a) Yarkovsky detection opportunities. I. Solitary asteroids. *Icarus, 173,* 166–184.

Vokrouhlický D., Čapek D., Chesley S. R., and Ostro S. J. (2005b) Yarkovsky detection opportunities. II. Binary asteroids. *Icarus, 179,* 128–138.

Vokrouhlický D., Brož M., Bottke W. F., Nesvorný D., and Morbidelli A. (2006a) Yarkovsky/YORP chronology of asteroid families. *Icarus, 182,* 118–142.

Vokrouhlický D., Brož M., BottkeW. F., Nesvorný D., and Morbidelli A. (2006b) The peculiar case of the Agnia asteroid family. *Icarus, 183,* 349–361.

Vokrouhlický D., Brož M., Morbidelli A., Bottke W. F., Nesvorný D., Lazzaro D., and Rivkin A. S. (2006c) Yarkovsky footprints in the Eos family. *Icarus, 182,* 92–117.

Vokrouhlický D., Nesvorný D., and BottkeW. F. (2006d) Secular spin dynamics of inner main-belt asteroids. *Icarus, 184,* 1–28.

Vokrouhlický D., Breiter S., Nesvorný D., and Bottke W. F. (2007) Generalized YORP evolution: Onset of tumbling and new asymptotic states. *Icarus, 191,* 636–650.

Vokrouhlický D., Chesley S. R., and Matson R. D. (2008) Orbital identification for asteroid 152563 (1992 BF) through the Yarkovsky effect. *Astron. J., 135,* 2336–2340.

Vokrouhlický D., Ďurech J., Michałowski T., et al. (2009) Datura family: The 2009 update. *Astron. Astrophys., 507,* 495–504.

Vokrouhlický D., Nesvorný D., Bottke W. F., and Morbidelli A. (2010) Collisionally born family about 87 Sylvia. *Astron. J., 139,* 2148–2158.

Vokrouhlický D., Ďurech J., Polishook D., et al. (2011) Spin vector and shape of (6070) Rheinland and their implications. *Astron. J., 142,* 159.

Vokrouhlický D., Farnocchia D., Čapek D., et al. (2015) The Yarkovsky effect for 99942 Apophis. *Icarus, 252,* 277–283.

Vraštil J. and Vokrouhlický D. (2015) Slivan states in the Flora region? *Astron. Astrophys., 579,* A14.

Walsh K. J., Richardson D. C., and Michel P. (2008) Rotational breakup as the origin of small binary asteroids. *Nature, 454,* 188–191.

Yarkovsky I. O. (1901) The density of luminiferous ether and the resistance it offers to motion (in Russian). Bryansk, published privately by the author.

Žižka J. and Vokrouhlický D. (2011) Solar radiation pressure on (99942) Apophis. *Icarus, 211,* 511–518.